A Section 508–conformant HTML version of this article is available at https://doi.org/10.1289/EHP3281.

Signaling Events Downstream of AHR Activation That Contribute to Toxic Responses: The Functional Role of an AHR-Dependent Long Noncoding RNA (*slincR*) Using the Zebrafish Model

Gloria R. Garcia, Prarthana Shankar, Cheryl L. Dunham, Abraham Garcia, Jane K. La Du, Lisa Truong, Susan C. Tilton, and Robert L. Tanguay

Department of Environmental and Molecular Toxicology, Sinnhuber Aquatic Research Laboratory, Environmental Health Sciences Center, Oregon State University, Corvallis, Oregon, USA

Background: A structurally diverse group of chemicals, including dioxins [e.g., 2,3,7,8-tetrachlorodibenzo-*p*-dioxin (TCDD)] and polycyclic aromatic hydrocarbons (PAHs), can xenobiotically activate the aryl hydrocarbon receptor (AHR) and contribute to adverse health effects in humans and wildlife. In the zebrafish model, repression of *sox9b* has a causal role in several AHR-mediated toxic responses, including craniofacial cartilage malformations; however, the mechanism of *sox9b* repression remains unknown. We previously identified a long noncoding RNA, *sox9b* long intergenic noncoding RNA (*slincR*), which is increased (in an AHR-dependent manner) by multiple AHR ligands and is required for the AHR-activated repression of *sox9b*.

Objective: Using the zebrafish model, we aimed to enhance our understanding of the signaling events downstream of AHR activation that contribute to toxic responses by identifying: *a*) whether *slincR* is enriched on the *sox9b* locus, *b*) *slincR*'s functional contributions to TCDD-induced toxicity, *c*) PAHs that increase *slincR* expression, and *d*) mammalian orthologs of *slincR*.

Methods: We used capture hybridization analysis of RNA targets (CHART), qRT-PCR, RNA sequencing, morphometric analysis of cartilage structures, and hemorrhaging screens.

Results: The *slincR* transcript was enriched at the 5′ untranslated region (UTR) of the *sox9b* locus. Transcriptome profiling and human ortholog analyses identified processes related to skeletal and cartilage development unique to TCDD-exposed controls, and angiogenesis and vasculature development unique to TCDD-exposed zebrafish that were injected with a splice-blocking morpholino targeting *slincR*. In comparison to TCDD exposed control morphants, *slincR* morphants exposed to TCDD resulted in abnormal cartilage structures and a smaller percentage of animals displaying the hemorrhaging phenotype. In addition, *slincR* expression was significantly increased in six out of the sixteen PAHs we screened.

Conclusion: Our study establishes that in zebrafish, *slincR* is recruited to the *sox9b* 5′ UTR to repress transcription, can regulate cartilage development, has a causal role in the TCDD-induced hemorrhaging phenotype, and is up-regulated by multiple environmentally relevant PAHs. These findings have important implications for understanding the ligand-specific mechanisms of AHR-mediated toxicity. https://doi.org/10.1289/EHP3281

Introduction

Recent advances in genetics and molecular biotechnology have resulted in a shift in the field of toxicology from observations of apical end points to investigations of the molecular initiating events in the adverse outcome pathway (National Research Council 2007). The aryl hydrocarbon receptor (AHR) is a conserved ligand-dependent transcription factor that is a member of the basic helix-loop-helix-PER-ARNT-SIM protein family. The AHR is known to be xenobiotically activated by a structurally diverse group of chemicals, including dioxins and polycyclic aromatic hydrocarbons (PAHs; Denison and Nagy 2003; Hahn et al. 2017). Upon ligand binding, the AHR translocates to the nucleus and heterodimerizes with the aryl hydrocarbon nuclear translocator (ARNT), inducing ligand-specific transcriptional changes (Beischlag et al. 2008). In vertebrates, the AHR also plays key roles in regulating a variety of physiological responses, such as immune and developmental processes, suggesting that too little or too much AHR activity can lead to adverse health effects (Esser and Rannug 2015; Murray et al. 2014). In zebrafish, the activation of the AHR by 2,3,7,8-tetrachlorodibenzo-*p*-dioxin (TCDD) and numerous PAHs results in the dysregulation of hundreds of genes and is associated with lethality, wasting, hemorrhaging, and defects in the skeletal and cardiovascular systems (Chlebowski et al. 2017; Denison and Nagy 2003; Garcia et al. 2018; Goodale et al. 2015).

The best-characterized high-affinity ligand used to study AHR-dependent toxicity is TCDD, a halogenated aromatic hydrocarbon. TCDD and related halogenated aromatic hydrocarbons are extremely toxic to most vertebrate species. The developmental zebrafish is among the most sensitive vertebrate models, making it ideal for investigating AHR signal transduction and function (Tanguay et al. 1999). *Ahr*-knockout mice and zebrafish mutants have demonstrated that the AHR is required for TCDD-induced toxicity (Fernandez-Salguero et al. 1995; Garcia et al. 2018; Goodale et al. 2012). In zebrafish, Ahr2 and Arnt1 are the functional orthologs of mammalian AHR and ARNT (Antkiewicz et al. 2006; Carney et al. 2006). Mammals and zebrafish share many toxic responses due to their well-conserved genomes, cell types, tissues, and organ systems (Garcia et al. 2016; Howe et al. 2013). Although the majority of downstream genes responsible for specific phenotypes of AHR-dependent toxicity remain largely unknown, the zebrafish model has been used to identify repression of *sox9b* as a key element responsible for producing craniofacial malformations, and to a lesser extent, cardiovascular malformations (Hofsteen et al. 2013; Xiong et al. 2008). Cardiovascular and craniofacial malformations are hallmarks of TCDD-induced developmental toxicity in fish and mammals (Couture et al. 1990; Henry et al. 1997). SOX9 (human ortholog of zebrafish Sox9b) is a conserved transcription factor that acts as the master regulator of cartilage development (Akiyama et al. 2002).

Address correspondence to R. L. Tanguay, Dept. of Environmental and Molecular Toxicology, Sinnhuber Aquatic Research Laboratory, Oregon State University, 28645 East Hwy 34, Corvallis, OR 97333 USA. Telephone: (541) 737-6514. FAX: (541) 737-0497. Email: robert.tanguay@oregonstate.edu

Supplemental Material is available online (https://doi.org/10.1289/EHP3281).

The authors declare they have no actual or potential competing financial interests.

Received 21 December 2017; Revised 15 October 2018; Accepted 16 October 2018; Published 6 November 2018.

The mechanism by which AHR activation leads to the repression of *sox9b* and subsequent developmental toxicities is still unknown; however, we have previously reported the identification of a long noncoding RNA (*sox9b* long intergenic noncoding RNA, *slincR*) that is up-regulated by multiple Ahr2 ligands and is located adjacent to *sox9b* (Garcia et al. 2017). Long noncoding RNAs (lncRNAs) are defined as transcripts equal to or greater than 200 base pairs (bps) long that do not appear to code for proteins. LncRNAs regulate an array of biological processes, including development, response to stress, embryonic viability, and cancer progression (Gutschner and Diederichs 2012; Li and Chang 2014; Nakagawa 2016). We have used two independent *ahr2*-mutant zebrafish lines ($ahr2^{hu3335}$ and $ahr2^{osu1}$) to demonstrate that *ahr2* is required for the TCDD-induced increase in *slincR* expression (Garcia et al. 2017; Garcia et al. 2018). Furthermore, *ahr2*-null zebrafish exposed to TCDD do not display a significant increase in *slincR*; *slincR* is required for typical tissue-specific expression of *sox9b* during normal development and is expressed in tissues with *sox9b*-essential functions, such as the jaw and snout regions, eyes, and brain (Garcia et al. 2017). Importantly, *slincR* expression is also required for the TCDD-induced repression of *sox9b*.

PAHs can activate the AHR and are ubiquitous environmental contaminants that are primarily created during the incomplete combustion of organic material (e.g., wood, coal, petrol, and oil; Shen et al. 2013). PAHs are of major concern due to their prevalence and potential toxic effects on ecosystems and human health (Perera 1997). PAHs can be genotoxic and/or carcinogenic, and *in utero* exposure has been associated with adverse birth outcomes (Boström et al. 2002; Dejmek et al. 2000; Perera et al. 2005). In human cohorts from urban environments, prenatal exposure to PAHs has also been associated with increased asthma prevalence and impaired cognitive development in offspring (Edwards et al. 2010; Tang et al. 2012).

The present study is broken down into the following four parts: "PART I: Transcriptional Regulation by *slincR*," "PART II: *slincR* Contributions to TCDD Toxicity," "PART III: Investigation of PAHs That Increase *slincR* Expression," and "PART IV: Identification of Potential *slincR* Mouse and Human Orthologs." In "PART I: Transcriptional Regulation by *slincR*," we investigated the mechanism of *slincR* repression of *sox9b* using capture hybridization analysis of RNA targets (CHART) to determine if *slincR* is enriched at the *sox9b* locus. We hypothesized that *slincR* binds (indirectly or directly) to the *sox9b* locus to repress *sox9b* expression, which contributes to the TCDD-induced cartilage malformation phenotype. We used a previously published *sox9b* morpholino to determine whether *sox9b* expression regulates the expression of *slincR*. We also analyzed the concentration–response relationship between developmental TCDD exposure and the gene expression of *sox9b* and *slincR*. In "PART II: *slincR* Contributions to TCDD Toxicity," to investigate *slincR*'s role in the TCDD-induced toxicity pathway, we performed RNA sequencing (RNA-seq) and Gene Ontology (GO) term enrichment analyses on 48-h post fertilization (hpf) control and *slincR* morphants exposed to 0.1% DMSO or 1 ng/mL TCDD. We hypothesized that with the reduction/absence of *slincR* expression (*slincR* morphants), there will be a relief in *sox9b* repression, and cartilage-associated GO processes will fail to be significantly enriched. To investigate the phenotypic impact of *slincR* expression on TCDD-induced jaw malformations, we measured the cartilage of 72-hpf control and *slincR* morphants treated with 0.1% DMSO or 1 ng/mL TCDD as described in Xiong et al. (2008). Due to the GO term enrichment of angiogenesis and vasculature-related processes in the *slincR* morphants, we performed a hemorrhaging screen on TCDD-exposed zebrafish at 48 hpf. For both the cartilage and hemorrhaging phenotypic analyses, we hypothesized that the *slincR* morphants exposed to TCDD will have a less severe toxicity phenotype and/or will be significantly different in comparison with the control morphant datasets. In "PART III: Investigation of PAHs That Increase *slincR* Expression," we determined if *slincR* expression was affected in response to sixteen different environmentally relevant PAHs. Finally, in "PART IV: Identification of Potential *slincR* Mouse and Human Orthologs," we mined multiple RNA-seq datasets to identify the potential mouse and human orthologs of *slincR*.

Materials and Methods

All gene-specific primers and probes were obtained from Integrated DNA Technologies and are listed in Supplemental Material, Table S1.

Fish Husbandry

The Tropical 5D line of zebrafish (*Danio rerio*) were purchased from 5D Tropical, Inc. The animals were reared according to Institutional Animal Care and Use Committee protocols at the Sinnhuber Aquatic Research Laboratory, Oregon State University. Adult fish were raised in a recirculating water system ($28 \pm 1°C$) with a 14-h:10-h light:dark schedule. Adult fish were fed GEMMA Micro 300 or 500 (Skretting, Inc.) twice a day. Larval and juvenile fish were fed GEMMA Micro 75 and 150, respectively, thrice a day (Barton et al. 2016). Spawning and embryo collection were conducted as described in Westerfield (2007). Briefly, zebrafish were housed in densities of ~ 500 fish per 50-gallon tank in recirculating water supplemented with Instant Ocean salts at 28°C. The embryos were collected using a spawning funnel, staged, and maintained in an incubator at 28°C.

Waterborne Exposure

Shield-stage (~ 6 hpf) embryos were exposed to 0, 0.0625, 0.125, 0.25, 0.5, or 1 ng/mL TCDD (311 nM, 95.3% purity; SUPELCO Solutions Within) or vehicle (0.1% DMSO) with gentle rocking for 1 h in 20-mL glass vials (10 embryos/mL). The 1-h duration of TCDD exposure was previously shown sufficient to produce the full TCDD-induced toxicity phenotypes (Henry et al. 1997). The 1 ng/mL concentration was selected to match our previously published TCDD exposure paradigm and results in 99–100% of 120-hpf zebrafish displaying the expected TCDD-induced toxicity phenotype (e.g., cartilage and heart malformations and edema) and an approximate $\log_2$(fold change) of -1 in *sox9b* expression (Garcia et al. 2017; Mathew et al. 2008). We know that TCDD partitions quickly into the embryonic compartment, and the half-life of TCDD is quite long due to a lack of metabolism; thus, this 1 ng/mL TCDD exposure paradigm is sufficient to fully activate the AHR (DeVito and Birnbaum 1995). During the exposures, vials were also gently inverted every 15 min to ensure proper mixing. Embryos were rinsed three times with embryo media and then raised in 100-mm Petri dishes (at 28°C) in approximately 50 mL of embryo media until collection at 48 hpf or 72 hpf, depending on the experimental assay. Embryo media consisted of 15 mM NaCl, 0.5 mM KCl, 1 mM $MgSO_4$, 0.15 mM KH_2PO_4, 0.05 mM Na_2HPO_4, and 0.7 mM $NaHCO_3$ (Westerfield 2000). The number of embryos raised in a Petri dish ranged from 10–50, depending on the subsequent assay.

Morpholino Injections

Expression levels were reduced using previously published splice-blocking morpholinos (MO) for *sox9b* (5′-TGCAGTAATTTACCGGAGTGTTCTC-3′), *slincR* (5′-GACCTAAACTCGACCTTACCAGATC-3′), and a standard negative control (5′-CCTCTTACCTCAGTTACAATTTATA-3′) obtained from Gene Tools,

LLC (Garcia et al. 2017; Xiong et al. 2008; Yan et al. 2005). The concentration of *slincR* morpholino used was demonstrated to produce no visible morphological effects and to knockdown *slincR* expression at ~98% and ~80% upon exposure to 0.1% DMSO or 1 ng/mL TCDD, respectively (Garcia et al. 2017). Approximately, 2 nL of a 1-mM [RNA-seq and quantitative real time polymerase chain reaction (qRT-PCR)] or 1.5-mM (cartilage morphometrics and hemorrhage screen) solution of *slincR* MO and control MO were microinjected into the yolk at the one-cell stage. Approximately 2 nL of a 1.9-mM solution of *sox9b* MO was microinjected into the yolk at the one-cell stage.

PART I: Transcriptional Regulation by slincR

qRT-PCR CHART. CHART is a method to identify lncRNA binding sites in the genome (Simon 2013). Zebrafish embryo preparation for CHART was adapted from Bogdanović et al. (2013), and CHART protocol and buffers are from Simon (2013). A detailed protocol is provided (Supplemental Material, S1: CHART Sample Preparation). In brief, zebrafish embryos were exposed to 0.1% DMSO or 1 ng/mL TCDD, as described above. At 24 hpf, embryos were dechorionated with pronase (31.77 μg/μL). At 48 hpf, embryos were screened for malformations, and the morphologically normal animals were euthanized by overdose of buffered tricaine methanesulfonate (MS-222, 200–300 mg/L) by prolonged immersion and monitored under a dissecting microscope until their hearts stopped beating (approximately 15 min). Whole 48-hpf zebrafish embryos were fixed with 4% PFA for 15 min at room temperature, and nuclei were isolated using a Dounce homogenizer and centrifugation. The isolated nuclei were crosslinked using 3.2% PFA and sonicated for 10 min in a Bioruptor® Pico with cycles of 30 s on and 30 s off. Further, 108 pmol of a 60-bp biotin-labeled capture probe targeting exon 1 of *slincR* was added to 100 μL of the sonication solution and incubated overnight at room temperature on an end-over-end rotator. The control probe comprised of the sense sequence of the same region, and the input samples did not contain a hybridization probe. The capture probes were washed four times with wash buffer and captured using Dynabeads™ MyOne™ Streptavidin T1 (Thermo Fisher Scientific, cat. no. 65601). The input sample was set aside during the washing phase. The samples were de-cross-linked using proteinase K (Ambion™, Thermo Fisher Scientific, cat. no. AM2548) and incubated at 55°C for 1 h, followed by 1 h and 40 min at 65°C. The enriched DNA and RNA were isolated using the ZYMO ZR-Duet™ DNA/RNA miniprep kit (cat. no. D7001) according to manufacturer's instructions. To determine *slincR* enrichment, 2 μL of RNA pull down was converted to cDNA using a SuperScript™ VILO™ cDNA synthesis kit (Thermo Fisher Scientific, cat. no. 11754050) according to manufacturer's instructions. The genomic DNA pull down was used to determine if *slincR* is enriched at the *sox9b* locus. Both the cDNA and genomic DNA enrichment were diluted at 1:20 and were analyzed with primers targeting the *slincR* transcript and *sox9b* locus via qRT-PCR using SYBR® green PCR master mix (Thermo Fisher Scientific, cat. no. 4312704) according to manufacturer's instructions.

Data analysis. Each condition had 3 biological replicates, where 1 replicate consisted of approximately 500 48-hpf zebrafish. The qRT-PCR data were first normalized to 1% input control, such that 6.644 cycles (i.e. dilution factor $\log_2(100)$) was subtracted from the cycle threshold value (CT; i.e., number of PCR replication cycles required for the sample signal to exceed background levels) of the diluted input and used to calculate the ΔCT for the two probe sets ($\Delta CT = CT[\text{probe}] - CT[1\%\ \text{input-6.644}]$). For DNA fold enrichment, we next adjusted relative to the sense probe ($\Delta\Delta CT = \Delta CT[\textit{slincR}\text{-probe}] - \Delta CT[\text{sense-probe}]$), and then fold enrichment was calculated ($2^{-\Delta\Delta CT}$). The RNA yield was calculated using the following equation ($2^{-\Delta\Delta CT} \times 100\%$). We assigned samples that did not amplify (no enrichment) a CT value of 40. The data were graphed using GraphPad Prism 7.02 software. The products were also analyzed via 1.2% agarose gel electrophoresis.

RNA extraction and mRNA quantification. Total RNA was extracted from 48-hpf whole embryos using RNAzol® (Molecular Research Center, Inc.) and a bullet blender with 0.5 mM zirconium oxide beads, (Next Advance) as recommended by the manufacturer. The RNA was purified using the Direct-zol MiniPrep kit (Zymo Research) and included an in-column DNase 1 digestion. RNA quality and quantity were assessed using a BioTek® Synergy™ Mx microplate reader with the Gen5™ Take3™ module.

For the *sox9b*-MO experiment, total RNA (500 ng) was reverse transcribed into cDNA with random primers using the ABI High-Capacity cDNA Reverse Transcription Kit (Thermo Fisher). In addition, qRT-PCR was performed using a StepOnePlus™ Real-Time PCR System (Applied Biosystems). The 20 μL reactions consisted of 10 μL 2X SYBR® Green Master Mix (Applied Biosystems), 0.4 μL each of 10 μM forward and reverse primers, and 15 ng cDNA. Expression values were normalized to β-actin and analyzed with the $2^{-\Delta\Delta CT}$ method as described in Livak and Schmittgen (2001). We used the following calculation to determine morpholino knockdown efficiencies: $\%KD = (1 - 2^{-\Delta\Delta CT}) \times 100\%$.

Statistical analysis. Each biological sample consisted of RNA from 20 pooled 48-hpf zebrafish with 4 biological replicates per condition ($n = 4$). Results were statistically analyzed and graphed with GraphPad Prism (version 7), and significance was determined using a one-way ANOVA with Tukey post hoc test or Kruskal-Wallis test with Dunn's post hoc test for data that passed or failed normality using the Shapiro-Wilk test, respectively.

For the concentration–response experiment, zebrafish embryos were exposed to six concentrations of TCDD (0, 0.0625, 0.125, 0.25, 0.5, and 1.0 ng/mL) at the shield stage as described in the "Waterborne Exposure" section of the "Methods." The 10–μL one-step qRT-PCR reactions were set up consisting of 5 μL SYBR® Green Master Mix and 0.08 μL reverse transcriptase enzyme mix (*Power* SYBR® Green RNA-to-CT™ 1-Step Kit; Applied Biosystems), 0.2 μL each of 10 μM forward and reverse primers, and 15 ng RNA per reaction. The QuantStudio 5 Real-Time PCR System (Thermo Fisher Scientific) was used under the following cycling conditions: reverse transcription at 48°C for 30 min, denaturation and activation of SYBR® polymerase at 95°C for 10 min, followed by 40 cycles of amplification (95°C for 15 s, 60°C for 1 min). Expression values were normalized to β-actin and analyzed with the $2^{-\Delta\Delta CT}$ method as described in Livak and Schmittgen (2001). The 0 ng/mL TCDD concentration served as the calibrator.

Statistical analysis. Each sample consisted of RNA from 20 pooled 48-hpf zebrafish with 4 biological replicates per condition. Results were statistically analyzed using R (version 3.4.1) in the RStudio (version 1.0.143) integrated development environment (IDE; R version 3.4.1; R Development Core Team; RStudio Team 2016). The data were $\log_2$-transformed and initially assessed for equal variance and normality using Levene's test and the Shapiro-Wilk test, respectively. Statistical significance was determined using a one-way ANOVA with a Dunnett post hoc test ($n = 4$, $p < 0.001$) from the multcomp package (version 1.4-8), and the data were graphed using ggplot2 (version 3.0.0; Hothorn et al. 2008; Wickham 2016).

Evaluation of mortality and 17 physical endpoints at *120 hpf*. Zebrafish embryos were exposed to six concentrations of TCDD (0, 0.0625, 0.125, 0.25, 0.5, 1.0 ng/mL) at the shield stage as described in the "Waterborne Exposure" section of the "Methods." The animals were loaded into round-bottom 96-well plates, with one embryo in 100 μL embryo media per well. We measured mortality and a suite of 17 end points (yolk sac edema,

body axis, eye, snout, jaw, otic vesicle, pericardial edema, brain, somite, pectoral fin, caudal fin, circulation, pigmentation, trunk length, swim bladder, notochord distortion, and alterations in touch response) at 120 hpf as described in Truong et al. (2014).

Statistical analysis. For each concentration, $n = 32$ across two 96-well plates (16 animals per plate per treatment group). The 0 ng/mL TCDD concentration served as the control. Due to the low category counts, the data were analyzed using a Fisher's exact test as it does not make distributional assumptions. To control for the family-wise error rate, we applied the Bonferroni correction for multiple comparisons ($p < 0.01$).

120-hpf larval photomotor response (LPR) assay. Zebrafish embryos were exposed to 0, 0.0625, or 0.125 ng/mL of TCDD at the shield stage ($\sim$6 hpf), as described in the "Waterborne exposure" section of the Methods. At 120 hpf, only embryos that were phenotypically normal underwent a larval photomotor response assay. The larval photomotor response was conducted using the ViewPoint Zebrabox system (ViewPoint Behavior Technology) as described in Knecht et al. (2017). Briefly, the LPR assay comprises 3-min alternating light and dark periods, for a total of four light:dark transitions. The first transition is counted as an acclimation period. The level was set at 525 LUX for the light period and integration time set to 6 s. Larval movement was recorded over each light:dark cycle, and average of total distance traveled per integration time point and area under the curve calculated.

Statistical analysis. For each concentration, $n = 32$ across two 96-well plates (16 animals per plate). The overall area under the curve for the final three light:dark transitions was computed for animals exposed to 0, 0.0625, or 0.125 ng/mL, and was compared with the 0 ng/mL TCDD concentration using a Kolmogorov-Smirnov test ($p \leq 0.01$).

PART II: slincR *Contributions to TCDD Toxicity*

TCDD RNA-seq sample preparation and analysis. RNA was extracted from control and *slincR* morphants exposed to 0.1% DMSO or 1 ng/mL TCDD at 48 hpf with 4 replicates per treatment group, as described above. RNA integrity was confirmed (RIN score >8) with an Agilent Bioanalyzer 2,100. Total RNA samples were sent to the Oregon State University Center for Genome Research and Biocomputing Core facilities for library preparation and sequencing. In addition, mRNA was poly A selected, and libraries were prepared with the PrepX™ mRNA and Illumina sequencing workflow (Wafergen Biosystems). Paired-end sequencing (150 bp) was conducted with an Illumina HiSeq® 3000 sequencer. Processing of next-generation sequencing (NGS) followed a pipeline for gene-level analysis (Anders et al. 2013). Briefly, reads were initially evaluated by FastQC (version 0.11.3) to detect major sequencing problems and quality control trimmed with Skewer (version 0.1.127) to remove ends of reads with low mean Phred quality score using options: `-mode pe -end-quality 30 -mean-quality 25 -format auto -threads 9` (Andrews 2015; Jiang et al. 2014). RNA-seq alignment and quantification proceeded with Bowtie2 (version 2.2.3) being used to build TopHat genome index files from the Genome Reference Consortium Zebrafish Build 10 (GRCz10) genome downloaded from Ensembl (release 89), ftp://ftp.ensembl.org/pub/release-89/fasta/danio_rerio/dna/Danio_rerio.GRCz10.dna.toplevel.fa.gz (Kim et al. 2013; Langmead et al. 2009; Langmead and Salzberg 2012). Trimmed reads were aligned with TopHat (version 2.1.1) using the following options optimized for trimmed, paired-end, stranded data: `-num-threads 9 -library-type fr-secondstrand -no-discordant -no-mixed -mate-inner-dist 20 -mate-std-dev 180 -min-anchor-length 5 -min-intron-length 10 -max-intron-length 400,000`. Samtools (version 1.4) was used to assess the percent of paired aligned reads and to sort aligned reads (binary alignment files, BAM) by name using the "`flagstat`" and "`sort -n -@9`" commands, respectively (Li et al. 2009). Gene counts were estimated using the htseq-count script from HTSeq (version 0.6.0) with the GRCz10 Ensembl (release 89) GTF annotation, ftp://ftp.ensembl.org/pub/release-89/gtf/danio_rerio/Danio_rerio.GRCz10.89.gtf.gz, and options: `-format=bam -idattr=gene_id -stranded=yes -mode=intersection-nonempty -order=name` (Anders et al. 2015).

Statistical analysis. Each biological sample consisted of RNA from 20 pooled 48-hpf zebrafish with 4 biological replicates per condition ($n = 4$). Differential expression analysis followed the maintained Bioconductor workflow developed by Y Chen et al. (2016), http://bioconductor.org/packages/release/workflows/vignettes/RnaSeqGeneEdgeRQL/inst/doc/edgeRQL.html, and was conducted using R (version 3.5.1; R Development Core Team), RStudio (version 1.1.453; RStudio Team), and a custom R script provided as a supplementary file (Differential_expression_custom_script.R; Supplemental Material, S2. Differential expression custom R script; (Huber et al. 2015). The Bioconductor package edgeR (version 3.22.3) was used to normalize counts and identify differentially expressed genes (Lun et al. 2016; McCarthy et al. 2012; Robinson and Smyth 2007, 2008; Robinson et al. 2010; Robinson and Oshlack 2010). Briefly, genes were filtered to exclude those with low counts across libraries, only keeping genes expressed in a minimum of four samples with average counts per million reads per sample above 0.82, which corresponds to a minimum read count of 10–20 (Y Chen et al. 2016; Lun et al. 2016). Filtered genes were then normalized across samples using the trimmed mean of M values (TMM) method to minimize composition bias between libraries (Robinson and Oshlack 2010). Differential expression of control vs. TCDD-exposed control or *slincR* morphants was determined with functions from edgeR, which uses the negative binominal generalized linear model extended by quasi-likelihood methods to fit the count data, the Cox-Reid profile-adjusted likelihood method to calculate dispersions, and empirical Bayes quasi-likelihood F-tests to calculate differential expression (Chen et al. 2014; Lun et al. 2016). The "robust = TRUE" option was used to protect the empirical Bayes estimates against the possibility of outlier genes with wide-ranging individual dispersions. Genes with a Benjamini-Hochberg (BH) adjusted $p \leq 0.05$ were considered significantly differentially expressed. The biomaRt package (version 2.36.1) was used to connect Ensembl gene ID information to Ensembl BioMart annotation information (e.g., gene symbols, biotypes, human orthologs, etc.), and heatmaps were created using the R package ComplexHeatmap (version 1.18.1; Durinck et al. 2005; Durinck et al. 2009; Gu et al. 2016). Heatmap clustering was derived from TMM-normalized, regular log-transformed gene values scaled by z-score (Love et al. 2016). To understand the functional consequences of TCDD exposure and *slincR* knockdown, we performed biological process network enrichment analysis and GO term enrichment on the significant differentially expressed human orthologs using GeneGo MetaCore (version 6.31 build 68930) from Clarivate Analytics as described in Haggard et al. (2016). Only enriched biological process networks and GO terms with a false discovery rate (FDR) adjusted $p \leq 0.05$ were considered significant. Sequencing data and processing details have been deposited in the NCBI Gene Expression Omnibus (GSE106131).

Cartilage staining and lower jaw cartilage morphometrics. Zebrafish embryos were microinjected with control and *slincR* MOs and exposed to 0.1% DMSO or 1 ng/mL TCDD, as described above. At 72 hpf, larvae were euthanized by overdose of buffered tricaine methanesulfonate (MS-222, 200–300 mg/L) by prolonged immersion and monitored under a dissecting microscope

until the hearts stopped beating (approximately 15 min). The animals were fixed in 4% paraformaldehyde overnight at 4°C. Pigmentation was removed by incubating fixed larval samples for 1 h in a mixture of 3% H_2O_2/1% KOH. The cartilage was stained with 0.4% Alcian Blue 8GX (Sigma-Aldrich) in 70% ethanol and 80 mM $MgCl_2$ as described in Walker and Kimmel (2007). Briefly, fixed animals were washed with PBS and dehydrated with an ethanol gradient. After removal of ethanol, the cartilage stain was added to larvae and rocked overnight at room temperature. The samples were washed with water and cleared using glycerol and KOH solutions. Larvae were imaged in 0.8% low-melt agarose at room temperature using a Keyence BZ-X700 at 10X with 0.45 aperture and processed with the BZ-X Analyzer software. Morphometric analysis ($n = 9$–10 embryos) of ventral larval pharyngeal cartilages was performed using ImageJ v1.51j8 and two customized macros (Customized_Set_Origin_Tool.ijm; Customized_Click_Coordinates_Tool.ijm; Supplemental Material, S3. Customized Set Origin Tool and S4. Customized Click Coordinates Tool), as described in Xiong et al. (2008).

Statistical analysis. Biological replicates consisted of 9–10 individual 72-hpf zebrafish measurements per treatment group. Statistical significance ($n = 9$ or 10, $p < 0.05$) was determined in RStudio (version 1.1.453) with the R (version 3.5.1; R Development Core Team) packages multcomp (version 1.4-8) and sandwich (version 2.4-0) using a modified one-way ANOVA and Tukey multiple comparison of means that is robust in regard to equal variance, sample sizes, and distribution, and data were graphed using ggplot2 (version 3.0.0), and a custom R script (Cartilage_morphometrics.R; Supplemental Material, S5. Cartilage morphometrics R script; Herberich et al. 2010; Hothorn et al. 2008; Wickham 2016; Zeileis 2004, 2006).

Hemorrhage screen. Zebrafish embryos were microinjected with control and *slincR* MOs and exposed to 0.1% DMSO or 1 ng/mL TCDD, as described above. At 48 hpf, the embryos were evaluated under a dissecting microscope for the presence or absence of hemorrhaging.

Statistical analysis. The DMSO and TCDD samples consisted of 3 or 5 biological replicates, respectively. Each biological replicate contained 10–12 individual 48-hpf zebrafish. Results were statistically analyzed with R (version 3.4.1; R Development Core Team) in the RStudio IDE (version 1.0.143; RStudio Team). The data were initially assessed for equal variance and normality using Levene's test and the Shapiro-Wilk test, respectively. Statistical significance ($n = 3$ or 5, $p < 0.001$) was determined using the Type III one-way ANOVA for unbalanced experimental designs from the car package (version 3.0-0) with a Tukey post hoc test from the multcomp package (version 1.4-8), and the data were graphed using ggplot2 (version 3.0.0; Fox and Weisberg 2011; Hothorn et al. 2008; Wickham 2016). The experiments were independently repeated a minimum of two times.

PART III: Investigation of PAHs That Increase slincR *Expression*

16 PAH RNA-seq sample preparation and analysis. The zebrafish embryos were exposed as described in Geier et al. (2018). Briefly, the chorions were enzymatically removed from 4-hpf zebrafish using a custom automated dechorionator. At 6 hpf, the embryos were placed into a 96-well round-bottom plate using automated embryo placement robots (Mandrell et al. 2012). Each well contained a single embryo and 100 µL embryo media. The 16 PAHs (Table 1) were analytical grade standards obtained from AccuStandard, Chiron Chemicals, and Santa Cruz Biotechnology. To make stock solutions, the 16 PAHs were dissolved in 100% DMSO. See Geier et al. (2018) for detailed stock information. A Hewlett Packard D300e chemical dispenser was used to expose the embryos in 96-well plates. To achieve optimal solution uniformity, the plates were sealed with Parafilm®, covered in foil, and shaken overnight at 235 rpm in an orbital shaker at 28°C (Truong et al. 2016). The exposure plates were then transferred to an incubator at 28°C for the duration of the exposure. The EC_{80}'s of the 16 PAHs were experimentally determined by the individual compound response. The 16 PAHs were first assessed at a wide range of concentrations (50, 35.6, 11.2, 5, and 1 µM, $n = 32$). Of the 16 PAHs, 9 did not result in morphological malformations and were subsequently tested at only 50 µM. The remaining 7 were tested using a definitive concentration range (11 concentrations, $n = 24$) determined between the highest concentration to not elicit any morphological effect and the lowest concentration that resulted in near 100% morbidity or mortality. The final EC_{80} concentrations tested are listed behind each chemical name in Table 1. Sigmoidal curves are often fit to concentration–response data.

Table 1. RNA sequencing gene expression results from zebrafish developmentally exposed to 16 PAHs from the shield stage to 48-hpf.

	cyp1a		*slincR*		*sox9b*	
Treatment	log_2FC	FDR	log_2FC	FDR	log_2FC	FDR
Retene (12.2 µM)	7.692	6.94×10^{-16}	3.006	2.50×10^{-10}	0.071	0.848
Benzo[*j*]fluoranthene (14.9 µM)	7.761	4.96×10^{-16}	3.922	9.65×10^{-14}	0.095	0.678
Benzo[*k*]fluoranthene[a] (1.9 µM)	7.913	2.91×10^{-16}	3.975	6.07×10^{-14}	0.168	0.792
Dibenzo[*a*,*h*]pyrene[a] (5 µM)	6.373	1.07×10^{-13}	2.936	1.09×10^{-9}	0.104	0.610
Dibenzo[*a*,*i*]pyrene (5 µM)	6.478	7.58×10^{-14}	2.785	5.17×10^{-9}	−0.191	0.811
Benzo[*b*]fluoranthene[a] (50 µM)	6.019	1.83×10^{-13}	2.139	4.25×10^{-6}	0.171	0.615
Fluoranthene[a] (50 µM)	3.142	1.40×10^{-6}	0.343	0.720	0.001	0.998
Phenanthrene[a] (50 µM)	2.093	0.0026	0.009	1.00	0.011	1.00
Acenapthene[a] (50 µM)	0.844	0.139	0.459	0.407	0.113	0.499
4*H*-cyclopenta[*def*]phenanthren-4-one (16.2 µM)	1.618	0.176	0.019	0.990	0.347	0.0664
Carbazole (50 µM)	2.126	0.0549	0.491	0.716	0.211	0.384
3-nitrofluoranthene (1.9 µM)	1.778	0.712	0.319	0.954	0.186	0.859
1,5-dimethylnaphthalene (50 µM)	0.806	1.00	0.401	1.00	0.003	1.00
9-methylanthracene (50 µM)	2.647	0.0091	0.711	0.411	0.140	0.511
2-methylnaphthalene (50 µM)	0.587	1.00	0.139	1.00	0.038	1.00
Anthracene[a] (50 µM)	2.467	0.366	1.083	0.415	0.137	0.632

Note: These data are part of an unpublished RNA sequencing dataset that was generated by Dr. M. Geier from the R. Tanguay laboratory. Concentrations were based on the EC_{80} and were experientially determined by the individual compound response. For the PAHs that did not elicit a morphological effect, the maximum soluble concentration tested (50 µM for most) was used. The Bioconductor package edgeR (statistical methodology based on the negative binomial distribution) was used to calculate the log_2FC and identify the significant differentially expressed genes ($n = 4$, BH-adjusted $p \leq 0.05$), when compared to the vehicle control (0.1% DMSO). BH, Benjamini-Hochberg; DMSO, dimethyl sulfoxide; FDR, BH-adjusted *p*-value; hpf, hours post fertilization; log_2FC, log_2(fold change); PAH, polycyclic aromatic hydrocarbon.
[a]Denotes a chemical that is one of the U.S. Environmental Protection Agency's 16 priority PAHs.

Here, we used a Hill Model (specifically a four-parameter log-logistic function) that was fit to the mean percentage of affected individuals for any morphological end point measured. All curves were fit with the drm() function from the drc package in R. This function uses least squares estimation to fit the curves. The Hill model was applied to estimate a concentration that caused 80% effects (EC_{80}). The computed EC_{80} was confirmed prior to conducting the RNA-seq. The data for the morphological effects of the 16 PAHs are reported in Geier et al. (2018).

Total RNA was isolated and quantified from pooled groups of eight 48-hpf zebrafish as described in the "RNA Extraction" section of the "Methods" section. Each treatment group contained 4 biological replicates. Total RNA samples were sent to Oregon State University Center for Genome Research and Biocomputing Core facilities for library preparation and sequencing. The 100-bp single-end read libraries were prepared using the Wafergen Robotic PolyA Enrichment Library Prep and Wafergen Robotic Stranded RNA Library Prep Kits. The samples were randomized across 6 lanes and sequenced using the Illumina HiSeq® 3000.

Statistical analysis. The reads were processed and analyzed as described in the "TCDD RNA-seq Sample Preparation and Analysis section" of the "Methods" section. Each biological sample consisted of RNA from 8 pooled 48-hpf zebrafish with 4 biological replicates per condition ($n = 4$, BH-adjusted $p \leq 0.05$).

PART IV: Identification of Potential slincR *Mouse and Human Orthologs*

Mouse TCDD-exposed dataset. All procedures were approved by the University of Wisconsin Animal Care and Use Committee and conducted in accordance with the National Institutes of Health (NIH) Guide for Care and Use of Laboratory Animals. Pregnant C57BL/6J mice were treated with 5 μg/kg TCDD on E13.5 following previously established protocols (Lin et al. 2003). At E16.75, dams were euthanized via CO_2 asphyxiation, and the urogenital sinuses (UGS) were dissected from fetuses as previously described (Branam et al. 2013). Each UGS was immediately placed into a 1.5-mL microfuge tube containing 300 μL of 1% trypsin (Difco, 215240) in PBS and incubated on ice for 30 min. Collagenase (Sigma C9891) was added to a final concentration of 1 mg/mL, followed by an additional 30–45 min incubation on ice. A dissecting microscope was used to mechanically separate UGS from fetal urogenital epitheliums (UGEs) after which the bladder and urethral epithelium were removed, leaving only UGE. Each treatment consisted of 3–4 biological replicates consisting of either 5 or 6 individual UGEs that were pooled for RNA isolation. Total RNA was purified from each UGE using the RNeasy® system (Qiagen) and analyzed using the Agilent Bioanalyzer 2100 and an Agilent RNA 6000 Pico Kit (Agilent Technologies). The samples were sequenced at the University of Wisconsin Madison Biotechnology Center, using an Illumina HiSeq® 2500. Processing of NGS was performed as described above in the "RNA sequencing analysis"' section with the following modifications: The genome index files were generated with the GRCm38 (Ensembl Release 87) genome file, ftp://ftp.ensembl.org/pub/release-87/fasta/mus_musculus/dna/Mus_musculus.GRCm38.dna.toplevel.fa.gz; reads were trimmed using the FASTX-Toolkit (version 0.0.13; http://hannonlab.cshl.edu/fastx_toolkit/index.html) with options: `fastx_trimmer -t 50 -Q 33`; TopHat2 options were `–library-type fr-unstranded –no-mixed –num-threads 10`; and gene counts were determined using the htseq-count script from HTSeq with the Ensembl Release 87 GTF annotation, ftp://ftp.ensembl.org/pub/release-87/gtf/mus_musculus/Mus_musculus.GRCm38.87.gtf.gz and options: `-f bam -i gene_id -m intersection-nonempty -s no`.

Statistical analysis. Each biological sample consisted of RNA from 5-6 pooled UGE tissue with 3–4 biological replicates per condition. The differential expression analysis was performed as described above in the RNA sequencing analysis section ($n = 3$–4, BH-adjusted $p \leq 0.05$).

Identification of potential mammalian* slincR *orthologs. The *slncky* Evolution Browser contains alignments and evolutionary metrics of lncRNAs conserved in the mouse (mm10, GRCm38) and human (hg38, GRCh38) genomes and was used to identify the potential human ortholog of *slincR* (Chen et al. 2016). We performed pairwise sequence alignments using the online global alignment tool Needle (EMBOSS) using the default settings (https://www.ebi.ac.uk/Tools/psa/). To compare tissue-specific expression, we downloaded RNA sequencing data from the National Center for Biotechnology Information BioProject database for the mouse, *2610035D17Rik* (BioProject: PRJNA66167; Gene ID: 72386), and human, *LINC00673* (BioProject PRJEB4337; Gene ID: 100499467), orthologs of *slincR*, as well as for *sox9* (BioProject: PRJNA66167; Gene ID: 100499467) and *SOX9* (BioProject PRJEB4337; Gene ID: 6662). The data were graphed using the R package ggplot2 (version 3.0.0; Fagerberg et al. 2014; Wickham 2016; Yue et al. 2014).

Results

PART I: Transcriptional Regulation by slincR

Use of qRT-PCR CHART to evaluate* slincR *enrichment at the* sox9b *locus. The *slincR* probe was shown to be capable of enriching the *slincR* transcript (Figure 1A) and was shown to be specific as demonstrated by the absence of the *slincR* transcript band in the sense probe samples of a representative 1.2% agarose gel (Figure 1B). We tested multiple regions of the *sox9b* promoter, and only the 5′ UTR of the promoter was consistently enriched in all three biological replicates in both the DMSO- and TCDD-treated samples (Figure 1C). The 5' UTR is also present in the *sox9b* transcript, so we tested the same region in CHART-isolated RNA; however, the RNA samples did not result in detectable amplification (no measurable enrichment).

To determine if *sox9b* expression levels have an effect on the expression of *slincR*, we microinjected single-cell zebrafish embryos with a splice-blocking morpholino targeting *sox9b* (*sox9b*-MO) or with a control morpholino (Con-MO) and collected RNA at 48 hpf. We used qRT-PCR to measure the relative expression levels of *sox9b* and *slincR*. The *sox9b*-MO reduced the levels of *sox9b* transcripts by 71% and resulted in a significant increase in *slincR* expression when compared with control morphants (Figure 1D).

To determine if a concentration–response relationship exists between the gene expression of *sox9b* and *slincR* in response to TCDD exposure, we developmentally exposed embryonic zebrafish to 0, 0.0625, 0.125, 0.25, 0.5, or 1.0 ng/mL of TCDD and measured the relative expression levels of *sox9b* and *slincR* in 48-hpf wild-type zebrafish. We also measured *cyp1a* expression as a marker of AHR activation. The expression levels of *slincR* and *cyp1a* were significantly elevated beginning at the 0.0625 ng/mL TCDD concentration and increased with increasing concentrations of TCDD, in comparison with 0 ng/mL TCDD (i.e., 0.1% DMSO; Figure 2A). The expression levels of *sox9b* were significantly decreased in the 0.5 and 1.0 ng/mL TCDD concentrations, in comparison with 0 ng/mL TCDD (Figure 2A).

In addition to gene expression changes, we also examined the embryos for developmental toxicity when exposed to the six concentrations of TCDD (0–1 ng/mL) using a 17 end point morphology screen at 120 hpf, as described in Truong et al. (2014). Developmental exposures of 0.25, 0.5, or 1.0 ng/mL TCDD induced significant malformations across multiple end points,

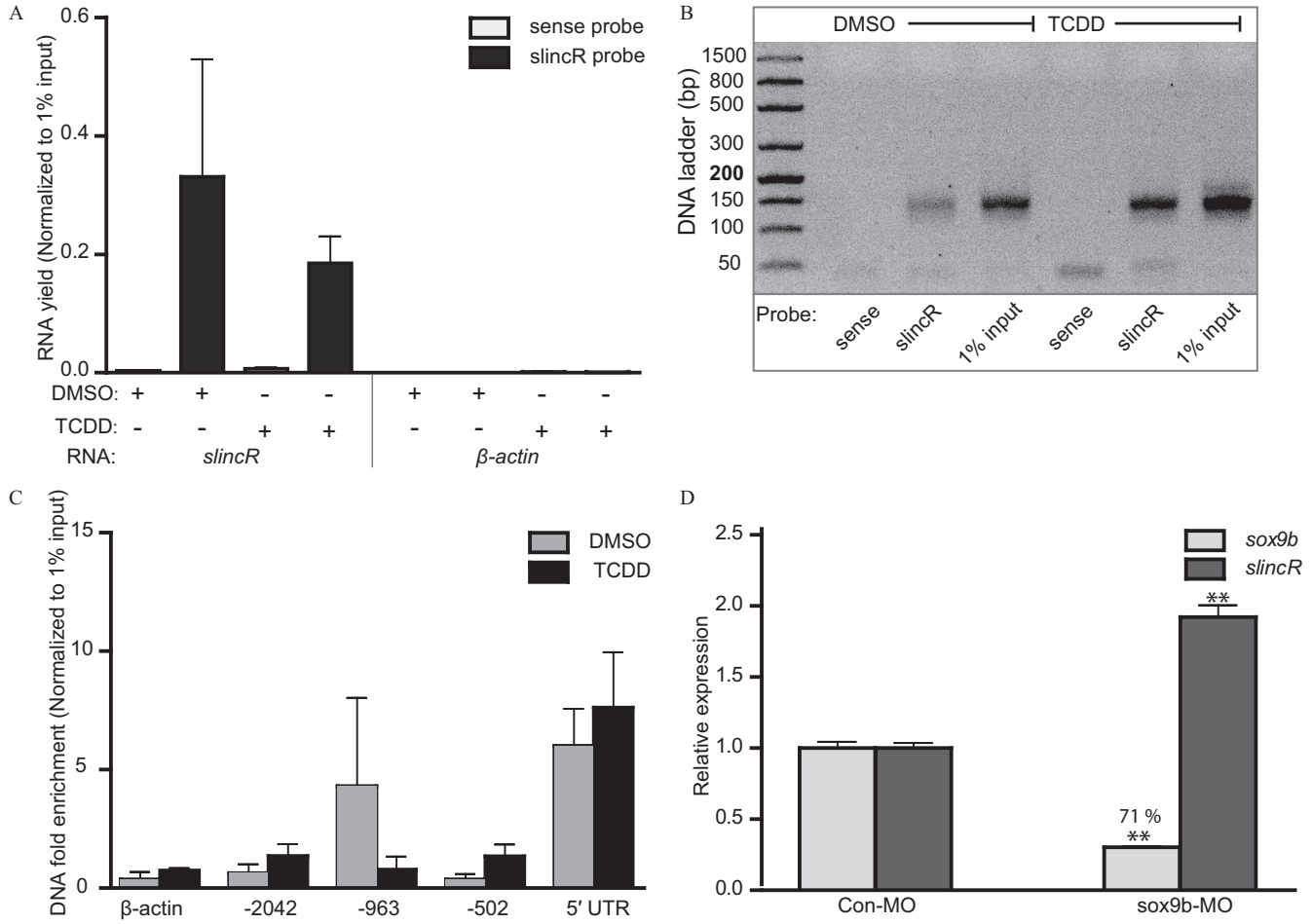

Figure 1. Use of qRT-PCR CHART to determine *slincR* enrichment at the *sox9b* promoter in 48-hpf whole embryos treated with 0.1% DMSO or 1 ng/mL TCDD. (*A*) Enrichment of *slincR* RNA by CHART (*slincR* probe) and a nonspecific primer set (β-actin). Each condition had 3 biological replicates, where 1 replicate consisted of approximately 500 48-hpf zebrafish. The qRT-PCR data were first normalized to 1% input control, such that 6.644 cycles (i.e., dilution factor $\log_2(100)$) was subtracted from the cycle threshold value (CT; i.e., number of PCR replication cycles required for the sample signal to exceed background levels) of the diluted input and used to calculate the ΔCT for the two probe sets (ΔCT = CT[probe] − CT[1% input-6.644]). The RNA yield was calculated using the following equation ($2^{-\Delta\Delta CT} \times 100\%$). We assigned samples that did not amplify (no enrichment) a CT value of 40. (*B*) Representative *slincR* qRT-PCR CHART products from panel (A) run on a 1.2% agarose gel. (*C*) qRT-PCR CHART enrichment of *slincR* RNA at multiple positions (−2042 bp, −963 bp, and −502 bp) downstream of the *sox9b* transcription start site and 5' untranslated region. Each condition had 3 biological replicates ($n = 3$), where 1 replicate consisted of approximately 500 48-hpf zebrafish. Expression values were normalized to 1% input control as described for panel (A), except for DNA fold enrichment. We next adjusted relative to the sense probe (ΔΔCT = ΔCT[*slincR*-probe] − ΔCT[sense-probe]), and then fold enrichment was calculated ($2^{-\Delta\Delta CT}$). We assigned samples that did not amplify (no enrichment) a CT value of 40. (*D*) qRT-PCR relative expression of *slincR* and *sox9b* mRNA in 48-hpf whole embryo control and *sox9b* morphants. Expression values were analyzed with the $2^{-\Delta\Delta CT}$ method and normalized to β-actin, whereas the control morphants served as the calibrator. Each sample represents a pool of 20 embryos, each condition had a minimum of four biological replicates ($n = 4$), and the data were analyzed using a one-way ANOVA with a Tukey post hoc test ($p < 0.01$ in comparison with control morphant = ∗∗). Error bars (A, C, and D) indicate standard error of the mean. Note: CHART, capture hybridization analysis of RNA targets; DMSO, dimethyl sulfoxide; hpf, hours post fertilization; TCDD, 2,3,7,8-tetrachlorodibenzo-*p*-dioxin; UTR, untranslated region.

including edemas (of the yolk and pericardium) and jaw, snout, eye, and pectoral fin malformations (Figure 2B, C). Developmental exposures of 0.0625 or 0.125 ng/mL did not induce a significant level of physical malformations (Figure 2B, C); however, both concentrations resulted in a significant hyperactive phenotype in a larval photomotor response (LPR) assay in comparison with 0 ng/mL TCDD (Figure 2D). Larval zebrafish exhibiting any visible malformation were necessarily excluded, which prevented the analysis of the 0.25, 0.5, or 1.0 ng/mL TCDD concentrations in the LPR assay.

PART II: slincR *Contributions to TCDD Toxicity*

Unbiased transcriptome profiling in TCDD-exposed zebrafish morphants. To gain insight into the functional role of *slincR* in TCDD-induced toxicity, we performed whole embryo transcriptome profiling on 48-hpf *slincR* and control morphants exposed to 0.1% DMSO or 1 ng/mL TCDD. In control morphants exposed to TCDD, we identified 132 genes that were differentially expressed when compared with vehicle control ($n = 4$, BH-adjusted $p \leq 0.05$, Figure 3A and Excel Table S1). In *slincR* morphants exposed to TCDD, we identified 80 differentially expressed genes when compared with vehicle control ($n = 4$, BH-adjusted $p \leq 0.05$, Figure 3A and Excel Table S2). Over 25% (22) of these genes were unique to *slincR* morphants, whereas 72.5% (58) overlapped with the control morphant differentially expressed gene list (Figure 3A). In the *slincR* and control morphant differentially expressed gene lists, 90% (72) and 81% (107) of the genes had an increase in expression in response to TCDD exposure, respectively. As expected, the *sox9b* transcript was only significantly decreased in the control morphant (TCDD-DMSO) dataset (Excel Table S1 and S2).

To visualize the expression profile, we performed bidirectional hierarchical clustering of the differentially expressed genes

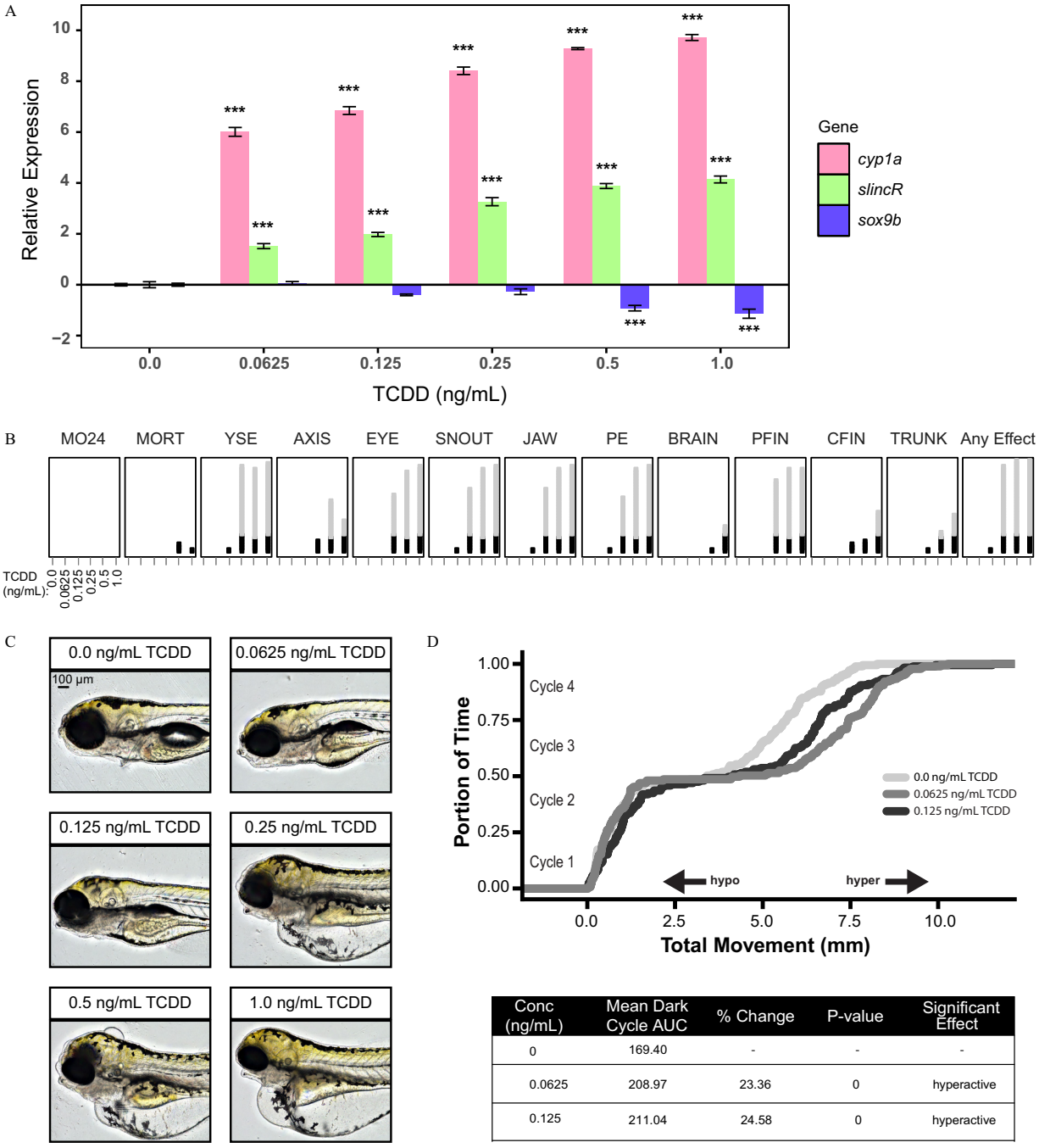

Conc (ng/mL)	Mean Dark Cycle AUC	% Change	P-value	Significant Effect
0	169.40	-	-	-
0.0625	208.97	23.36	0	hyperactive
0.125	211.04	24.58	0	hyperactive

Figure 2. Analysis of the concentration–response effects of developmental exposure (1-h exposure at 6 hpf) to TCDD on gene expression at 48 hpf and morphological malformations at 120 hpf. (*A*) qRT-PCR relative expression of *cyp1a*, *slincR*, and *sox9b* transcripts in 48-hpf wild-type embryos exposed to 0, 0.625, 0.125, 0.25, 0.5, or 1.0 ng/mL TCDD. For all assays, 0.1% DMSO served as the vehicle control and is listed as 0 ng/mL TCDD. Expression values were analyzed with the $2^{-\Delta\Delta CT}$ method and normalized to β-actin using the 0 ng/mL TCDD concentration as the calibrator. Each experimental unit represents a pool of 20 embryos, and each treatment group included four biological replicates ($n = 4$). The data were $\log_2$-transformed and analyzed using a one-way ANOVA with a Dunnett post hoc test ($p < 0.001$ in comparison with 0 ng/mL TCDD = ∗∗∗). All error bars indicate standard error of the mean. (*B*) Evaluation of 17 physical malformations at 120-hpf on wild-type zebrafish exposed to six concentrations of TCDD (0–1 ng/mL) across two 96-well plates. Nonsignificant malformations (otic vesicle, somite, circulation, pigmentation, swim bladder, notochord distortion, and alterations in touch response) are excluded. The horizontal axis displays the TCDD concentrations tested, and the malformation examined is listed above each box. The incidence across all replicates is plotted as stacked points. For each malformation, the stacked points exceeding the binomial significance threshold are represented in light gray (top stack). The data were analyzed using a Fisher's exact test with a Bonferroni correction for multiple comparisons ($n = 32$, $p < 0.01$). (*C*) Representative lateral images of 120-hpf zebrafish for each concentration of TCDD tested. The bar in top left corner indicates 100 µM. (*D*) Larval photomotor response (LPR) in 120-hpf wild-type embryos developmentally exposed to 0, 0.0625, or 0.125 ng/mL TCDD equally divided across two 96-well plates using the ViewPoint ZebraBox larvae screening system. For each concentration of TCDD, the overall area under the curve was analyzed for the last 3 light:dark cycles in comparison with 0 ng/mL TCDD using a Kolmogorov-Smirnov test ($n = 32$, $p \leq 0.01$). Note: AUC, area under the curve; AXIS, body axis; CFIN, caudal fin; Conc, concentration; cycle, 3-minute light:dark transitions; DMSO, dimethyl sulfoxide; hpf, hours post fertilization; hypo, hypoactive photomotor response; hyper, hyperactive photomotor response; MO24, mortality measured at 24 hpf; MORT, mortality measured at 120 hpf; PE, pericardial edema; PFIN, pec fin; TCDD, 2,3,7,8-tetrachlorodibenzo-*p*-dioxin; YSE, yolk sac edema.

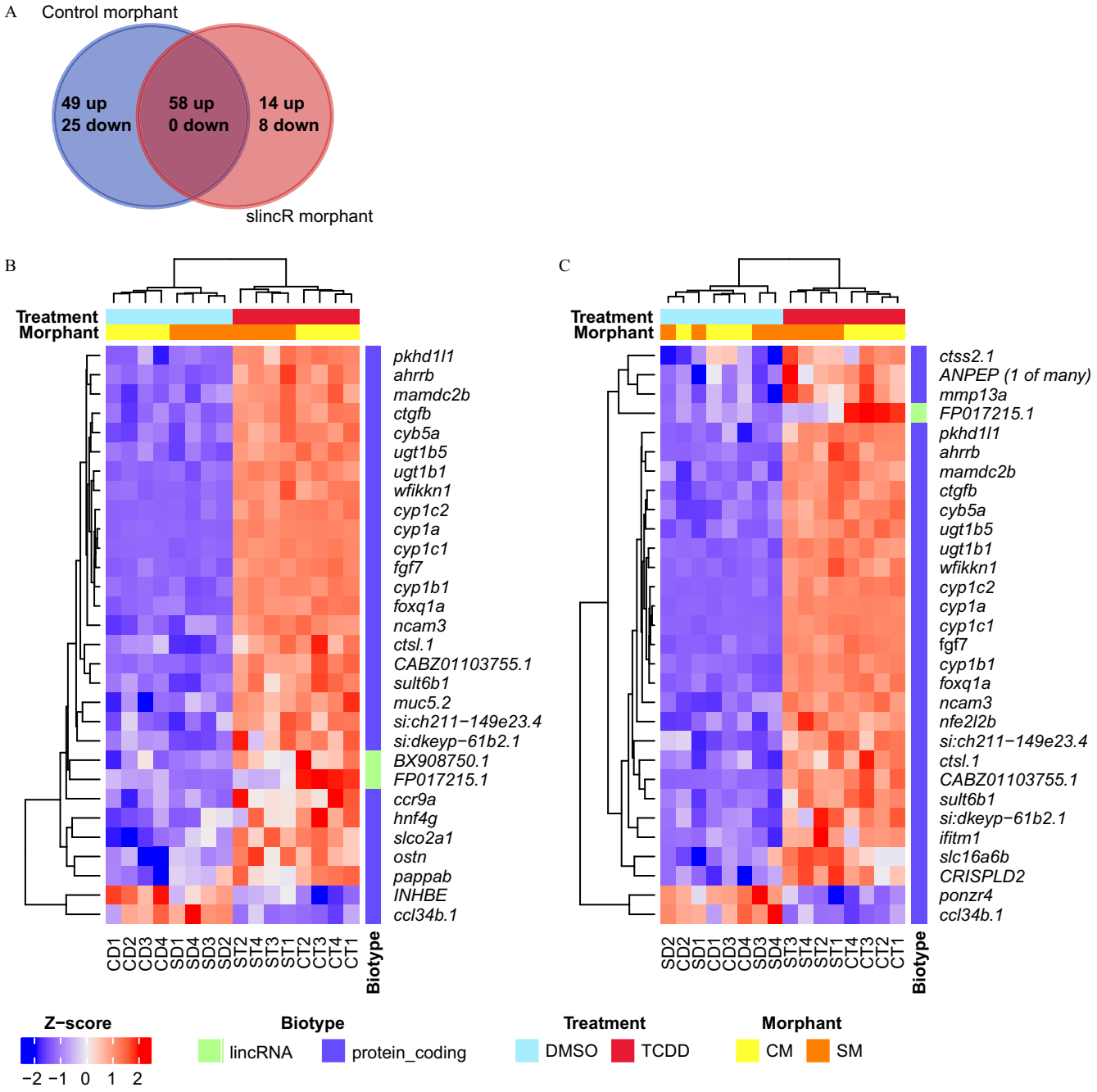

Figure 3. Venn diagram of all differentially expressed genes, and heatmaps of significantly differentially expressed genes with the top 30 largest $\log_2$(fold change) between 48-hpf *slincR* and control morphants treated developmentally (1 h exposure at 6 hpf) with 0.1% DMSO or 1 ng/ml TCDD. The Bioconductor package edgeR (statistical methodology based on the negative binomial distribution) was used to identify the significant differentially expressed genes in TCDD-treated morphants ($n = 4$, BH-adjusted $p \leq 0.05$), in comparison with the vehicle control (0.1% DMSO). (*A*) Venn diagram of up- and down regulated genes from control and *slincR* morphants. Hierarchical clustering is derived from TMM-normalized, regular log-transformed gene counts scaled by *z*-score as shown by heatmaps of (*B*) control morphant TCDD (CT) in comparison with control morphant DMSO (CD) and (*C*) *slincR* morphant TCDD (ST) in comparison with *slincR* morphant DMSO (SD). *slincR* is represented by the Ensembl gene symbol FP017215.1 in the heatmaps. Each condition included four biological replicates (i.e., CD1, CD2, CD3, and CD4), with each replicate representing a pool of 20 embryos. Note: BH, Benjamini-Hochberg; DMSO, dimethyl sulfoxide; TCDD, 2,3,7,8-tetrachlorodibenzo-*p*-dioxin.

with the top 30 largest $\log_2$(fold changes) in control (Figure 3B) and *slincR* (Figure 3C) morphants. TCDD exposure produced a robust transcriptional profile as indicated by the two primary transcript clusters that separate based on treatment status (blue and red bars at the top of the heatmaps).

To relate the observed transcriptional changes to human health and understand the functional consequences of TCDD exposure and *slincR* knockdown, we identified orthologous human Ensembl genes and performed biological process network enrichment and GO term enrichment analyses on the converted gene lists using MetaCore GeneGo software (FDR-adjusted $p \leq 0.05$) as described in Haggard et al. (2016). The MetaCore process network enrichment for the *slincR* morphant dataset was limited because of its small size but included four networks involved in immune response, regulation of epithelial-to-mesenchymal transition, ESR1-nuclear pathway, and reproduction, that were also

Table 2. Significantly enriched MetaCore process networks from 48-hpf Con-MO zebrafish developmentally exposed to 1 ng/mL TCDD for 1 h at the shield stage, compared to the vehicle control (0.1% DMSO).

Network name	FDR	Associated human gene
Development: Cartilage development	8.053×10^{-3}	*BMP4*, *BMP6*, *COL12A1*, *SOX9*, *CTGF*
Cell adhesion: Cell-matrix interactions	8.053×10^{-3}	*COL12A1*, *THBS1*, *MMP9*, *VCAN*, *ITGA11*, *TNC*, *COL10A1*
Immune response: Th17-derived cytokines	8.053×10^{-3}	*CXCL12*, *IL17RC*, *MMP9*, *JUN*
Development: Ossification and bone remodeling	8.053×10^{-3}	*BMP4*, *BMP6*, *OSTN*, *FOXO1*, *COL10A1*, *POSTN*
Signal Transduction: BMP and GDF signaling	8.053×10^{-3}	*BMP4*, *BMP6*, *CDKN1B*, *GADD45B*, *SOX9*
Development: EMT: Regulation of epithelial-to-mesenchymal transition	8.053×10^{-3}	*BMP4*, *HMGA2*, *MMP9*, *JUN*, *CDKN1B*, *SOX9*, *CTGF*
Proteolysis: ECM remodeling	8.053×10^{-3}	*MMP9*, *TNC*, *COL10A1*, *CTGF*
Signal Transduction: ESR1-nuclear pathway	9.733×10^{-3}	*CYP1A1*, *CXCL12*, *BMP6*, *ADM*, *JUN*, *FOXO1*, *CYP1B1*
Reproduction: FSH-beta signaling pathway	2.218×10^{-2}	*BMP4*, *JUN*, *FOXO1*, *CDKN1B*, *CTGF*
Development: Blood vessel morphogenesis	2.424×10^{-2}	*EPAS1*, *CXCL12*, *BMP4*, *FOXO1*, *CTGF*, *ANGPT4*

Note: The Bioconductor package edgeR (statistical methodology based on the negative binomial distribution) was used to calculate the significant differentially expressed genes ($n = 4$, BH-adjusted $p \leq 0.05$), in comparison with the vehicle control (0.1% DMSO). The human orthologs of the gene list were then submitted to MetaCore to identify significantly enriched process networks using a hypergeometric distribution, where the p-value is the probability that a gene set maps to a manually curated GeneGo Process Network or is overrepresented in comparison with the background gene list. Enriched process networks were considered significant with an FDR ≤ 0.05. BH, Benjamini-Hochberg; BMP, bone morphogenic protein; Con-MO, control morphant; DMSO, dimethyl sulfoxide; ECM, extracellular matrix; EMT, epithelial to mesenchyme transition; FDR, false discovery rate adjusted p-value; FSH-beta, follicle-stimulating hormone beta subunit; GDF, growth differentiation factor; hpf, hours post fertilization; slincR-MO, *slincR* morphant; TCDD, 2,3,7,8-tetrachlorodibenzo-*p*-dioxin.

significantly enriched in the control morphant data (Table 2 and 3). We observed multiple enriched process networks involved in cartilage, bone, and blood vessel development in the control morphant dataset. The GO term enrichment analyses resulted in about half of GO-enriched terms overlapping between Con-MO and *slincR*-MO datasets (Excel Table S3 and S4). We noticed that several cartilage and skeletal developmental processes were uniquely enriched in the control morphant data (Table 4), whereas angiogenesis and vasculature developmental processes were uniquely enriched in the *slincR* dataset (Table 5).

Effect of* slincR *knockdown on jaw development after treatment with TCDD. To investigate the phenotypic impact of *slincR* expression on TCDD-induced jaw malformations, we developmentally exposed *slincR* and control morphants to 0.1% DMSO or 1 ng/mL TCDD for 1 h at the shield stage ($\sim$6 hpf) and evaluated the cartilage of 72-hpf zebrafish larvae. Both the control and *slincR* morphants exposed to TCDD had a 100% incidence of cartilage malformations at 72 hpf. The cartilage of DMSO-exposed *slincR* and control morphants was indistinguishable; however, *slincR* morphants exposed to TCDD had a significant difference in the relative position of landmark structures in comparison with TCDD-exposed control morphants ($n = 9$ or 10, $p < 0.05$; Figure 4A, B). Unexpectedly, knocking down *slincR* expression in TCDD-exposed (Ahr2-activated) zebrafish embryos resulted in an abnormal junction between hyosymplectic and ceratohyal cartilages in comparison with control morphants exposed to TCDD (Figure 4B, region of interest indicated by arrows in trace column).

Effect of* slincR *knockdown on TCDD-induced hemorrhaging. To elucidate the phenotypic impact of *slincR* expression on TCDD-induced hemorrhaging, we developmentally exposed *slincR* and control morphants to 0.1% DMSO (vehicle control) or 1 ng/mL TCDD for 1 h at the shield stage ($\sim$6 hpf). At 48 hpf, the embryos were evaluated for the presence or absence of hemorrhaging as shown in (Figure 5A, B; blood pooling indicated by arrows). In control and *slincR* morphants, exposure to DMSO did not result in hemorrhaging (Figure 5A). In both the control and *slincR* morphants, exposure to TCDD resulted in a significant increase in the percent incidence of zebrafish displaying a hemorrhaging phenotype in comparison with their respective vehicle controls ($n = 3$ or 5, $p < 0.001$; Figure 5A); however, the *slincR* morphants exposed to TCDD had a significant decrease in the percentage of animals with the hemorrhaging phenotype in comparison with control morphants exposed to TCDD (Figure 5A).

PART III: Investigation of PAHs That Increase slincR *Expression*

slincR* *is up-regulated by multiple environmentally relevant PAHs. To screen for environmentally relevant PAHs that activate the AHR signaling pathway and up-regulate *slincR* expression, we mined an unpublished 16 PAH RNA-seq dataset from 48-hpf whole zebrafish embryos generated by Dr. M. Geier from the Tanguay lab. Of the 16 PAHs screened, six were associated with a significant increase in *cyp1a* and *slincR* expression, of which three were from the U.S. Environmental Protection Agency's priority PAH list (Table 1). Three additional PAHs were associated with a significant increase in *cyp1a* expression alone, of which two were from the EPA's priority PAH list. None of the 16 PAHs were associated with a significant decrease in *sox9b* expression.

PART IV: Identification of Potential slincR *Mouse and Human Orthologs*

To identify the potential mouse ortholog of *slincR*, we mined an unpublished RNA-seq dataset from male and female mouse E16.75 urogenital epithelial tissue exposed to 5 μg/kg of TCDD,

Table 3. Significantly enriched MetaCore process networks from 48-hpf slincR-MO zebrafish exposed to 1 ng/mL TCDD for 1 hour at the shield stage, in comparison with the vehicle control (0.1% DMSO).

Network name	FDR	Associated human gene
Immune response: Th17-derived cytokines	2.946×10^{-2}	*JUN*, *CXCL12*, *MMP9*
Development: EMT Regulation of epithelial-to-mesenchymal transition	2.946×10^{-2}	*JUN*, *CDKN1B*, *TWIST1*, *CTGF*, *MMP9*
Signal transduction: ESR1-nuclear pathway	2.946×10^{-2}	*CYP1A1*, *JUN*, *NFATC4*, *CXCL12*, *CYP1B1*
Reproduction: FSH-beta signaling pathway	2.946×10^{-2}	*JUN*, *CDKN1B*, *FST*, *CTGF*

Note: The Bioconductor package edgeR (statistical methodology based on the negative binomial distribution) was used to calculate the significant differentially expressed genes ($n = 4$, BH-adjusted $p \leq 0.05$), in comparison with the vehicle control (0.1% DMSO). The human orthologs of the gene list were then submitted to MetaCore to identify significantly enriched process networks using a hypergeometric distribution, where the p-value is the probability that a gene set maps to a manually curated GeneGo Process Network or is overrepresented in comparison with the background gene list. Enriched process networks were considered significant with an FDR ≤ 0.05. BH, Benjamini-Hochberg; DMSO, dimethyl sulfoxide; EMT, epithelial to mesenchyme transition; FDR, false discovery rate adjusted p-value; FSH-beta, follicle-stimulating hormone beta subunit; hpf, hours post fertilization; slincR-MO, *slincR* morphant; TCDD, 2,3,7,8-tetrachlorodibenzo-*p*-dioxin.

Table 4. Significantly enriched unique MetaCore GO processes related to skeletal and cartilage development from 48-hpf Con-MO zebrafish exposed to 1 ng/mL TCDD for 1 h at the shield stage, in comparison with the vehicle control (0.1% DMSO).

Biological process	FDR	Associated human gene
Ossification	7.152×10^{-5}	*CYP24A1*, *BMP4*, *BMP6*, *MMP9*, *OSTN*, *VCAN*, *ITGA11*, *TNC*, *SOX9*, *COL10A1*, *CTGF*
Cartilage development	2.601×10^{-4}	*BMP4*, *BMP6*, *HMGA2*, *THBS1*, *SFRP2*, *SOX9*, *COL10A1*, *CTGF*
Endochondral bone morphogenesis	1.968×10^{-3}	*BMP4*, *BMP6*, *THBS1*, *SOX9*, *COL10A1*
Osteoblast differentiation	4.093×10^{-3}	*CYP24A1*, *BMP4*, *BMP6*, *VCAN*, *ITGA11*, *TNC*
Bone development	5.122×10^{-3}	*BMP4*, *BMP6*, *THBS1*, *PAPPA2*, *SFRP2*, *SOX9*, *COL10A1*
Regulation of chondrocyte differentiation	5.710×10^{-3}	*BMP4*, *BMP6*, *SOX9*, *CTGF*
Chondrocyte differentiation	1.142×10^{-2}	*BMP4*, *HMGA2*, *SFRP2*, *SOX9*
Regulation of cartilage development	1.177×10^{-2}	*BMP4*, *BMP6*, *SOX9*, *CTGF*
Positive regulation of osteoblast differentiation	1.271×10^{-2}	*IL6R*, *BMP4*, *BMP6*, *SFRP2*
Regulation of osteoblast differentiation	1.324×10^{-2}	*IL6R*, *BMP4*, *BMP6*, *OSTN*, *SFRP2*
Regulation of bone mineralization	1.356×10^{-2}	*BMP4*, *BMP6*, *OSTN*, *SOX9*
Odontogenesis of dentin-containing tooth	1.356×10^{-2}	*BMP4*, *ADM*, *FOXO1*, *TNC*
Positive regulation of cartilage development	1.567×10^{-2}	*BMP4*, *BMP6*, *SOX9*
Regulation of biomineral tissue development	1.578×10^{-2}	*BMP4*, *BMP6*, *OSTN*, *SOX9*
Regulation of ossification	1.793×10^{-2}	*IL6R*, *BMP4*, *BMP6*, *OSTN*, *SFRP2*, *SOX9*
Chondrocyte proliferation	1.793×10^{-2}	*HMGA2*, *CTGF*
Endochondral ossification	2.003×10^{-2}	*BMP4*, *BMP6*, *COL10A1*
Replacement ossification	2.003×10^{-2}	*BMP4*, *BMP6*, *COL10A1*
Positive regulation of ossification	2.891×10^{-2}	*IL6R*, *BMP4*, *BMP6*, *SFRP2*
Odontogenesis	2.954×10^{-2}	*BMP4*, *ADM*, *FOXO1*, *TNC*
Negative regulation of chondrocyte differentiation	4.076×10^{-2}	*BMP4*, *SOX9*

Note: The Bioconductor package edgeR (statistical methodology based on the negative binomial distribution) was used to calculate the significant differentially expressed genes ($n = 4$, BH-adjusted $p \leq 0.05$), in comparison with the vehicle control (0.1% DMSO). The human orthologs of the gene list were then submitted to MetaCore to identify significant biological processes using a hypergeometric distribution, where the p-value is the probability that a gene set maps to a manually curated GO process or is overrepresented in comparison with the background gene list. Enriched GO processes were considered significant with an FDR ≤ 0.05. BH, Benjamini-Hochberg; Con-MO, control morphant; DMSO, dimethyl sulfoxide; FDR, false discovery rate adjusted p-value; GO, gene ontology; hpf, hours post fertilization; TCDD, 2,3,7,8-tetrachlorodibenzo-p-dioxin.

which was generated by the Richard Peterson lab from the University of Wisconsin-Madison. In the zebrafish genome, *slincR* is located adjacent and antisense to *sox9b*; therefore, we searched for a lncRNA that was significantly increased in response to TCDD and had a conserved genomic position and orientation relative to *Sox9* in the mouse genome. We identified a single lncRNA (*2610035D17Rik*) that matched these criteria (Figure 6A, B). We used the *slncky* Evolution Browser to search for the human ortholog of mouse *2610035D17Rik* and identified *LINC00673* (Figure 6C; Chen et al. 2016). A sequence comparison of the zebrafish *slincR* sequence (466 bp) with the mouse (1802 bp) and human (2275 bp) lncRNAs resulted in a 17.6% and 13.4% sequence identity, respectively. The mouse and human lncRNAs shared 43.1% sequence identity. To determine if the mouse and human lncRNAs have similar tissue-specific expression patterns in comparison with *slincR* in zebrafish, we downloaded mouse and human RNA-seq expression data from NCBI and graphed the expression of the potential *slincR* orthologs and *Sox9/SOX9* across multiple tissues (Figure 6D, E). Concordant with *slincR*, expression of both *2610035D17Rik* and *LINC00673* was found in the brain and central nervous system, and *2610035D17Rik* expression was also identified in the developing limb bud.

Discussion

The AHR is required for proper vertebrate development and homeostasis; however, activation of the receptor by ubiquitous environmental pollutants, such as PAHs, can lead to adverse developmental and cognitive effects in humans and wildlife (Carney et al. 2006; Schneider et al. 2014). Dysregulation of the AHR signal transduction pathway is associated with multiple diseases, including prostate and coronary artery disease (Huang et al. 2015; Schneider et al. 2014; Vezina et al. 2009). AHR dysregulation has also been implicated in many cancer types and mediates a number of steps in tumor progression (Murray et al. 2014; Opitz et al. 2011). Recent publications suggest the AHR may play a role in maintaining the cancer stemlike phenotype and may exert transcription-independent functions to mediate resistance to treatment in adenocarcinoma and nonsmall cell lung cancers, respectively (Yan et al. 2018; Ye et al. 2018).

A better understanding of the molecular mechanisms that lead to toxic outcomes will facilitate the necessary shift from observations of apical end points (e.g., malformations, mortality) to predicting the potential of a chemical to alter or interfere with biologically conserved pathways (Noyes et al. 2016). We

Table 5. Significantly-enriched unique MetaCore GO processes related to angiogenesis and vasculature development from 48-hpf slincR-MO zebrafish exposed to 1 ng/mL TCDD for 1 h at the shield stage, in comparison with the vehicle control (0.1% DMSO).

Biological process	FDR	Associated human gene
Regulation of blood vessel endothelial cell proliferation involved in sprouting angiogenesis	9.926×10^{-3}	*HMOX1*, *THBS1*
Negative regulation of vascular smooth muscle cell proliferation	1.297×10^{-2}	*CDKN1B*, *HMOX1*
Regulation of blood vessel endothelial cell migration	2.806×10^{-2}	*HMOX1*, *NFE2L2*, *THBS1*
Positive regulation of vascular smooth muscle cell proliferation	2.941×10^{-2}	*JUN*, *MMP9*
Positive regulation of blood coagulation	3.062×10^{-2}	*NFE2L2*, *THBS1*
Regulation of cell migration involved in sprouting angiogenesis	4.019×10^{-2}	*HMOX1*, *THBS1*
Branching involved in blood vessel morphogenesis	4.456×10^{-2}	*NFATC4*, *CXCL12*

Note: The Bioconductor package edgeR (statistical methodology based on the negative binomial distribution) was used to calculate the significant differentially expressed genes ($n = 4$, BH-adjusted $p \leq 0.05$), in comparison with the vehicle control (0.1% DMSO). The human orthologs of the gene list were then submitted to MetaCore to identify significant biological processes using a hypergeometric distribution, where the p-value is the probability that a gene set maps to a manually curated GO process or is overrepresented compared to the background gene list. Enriched GO processes were considered significant with an FDR ≤ 0.05. BH, Benjamini-Hochberg; DMSO, dimethyl sulfoxide; FDR, false discovery rate adjusted p-value; GO, gene ontology; hpf, hours post fertilization; slincR-MO, *slincR* morphant; TCDD, 2,3,7,8-tetrachlorodibenzo-p-dioxin.

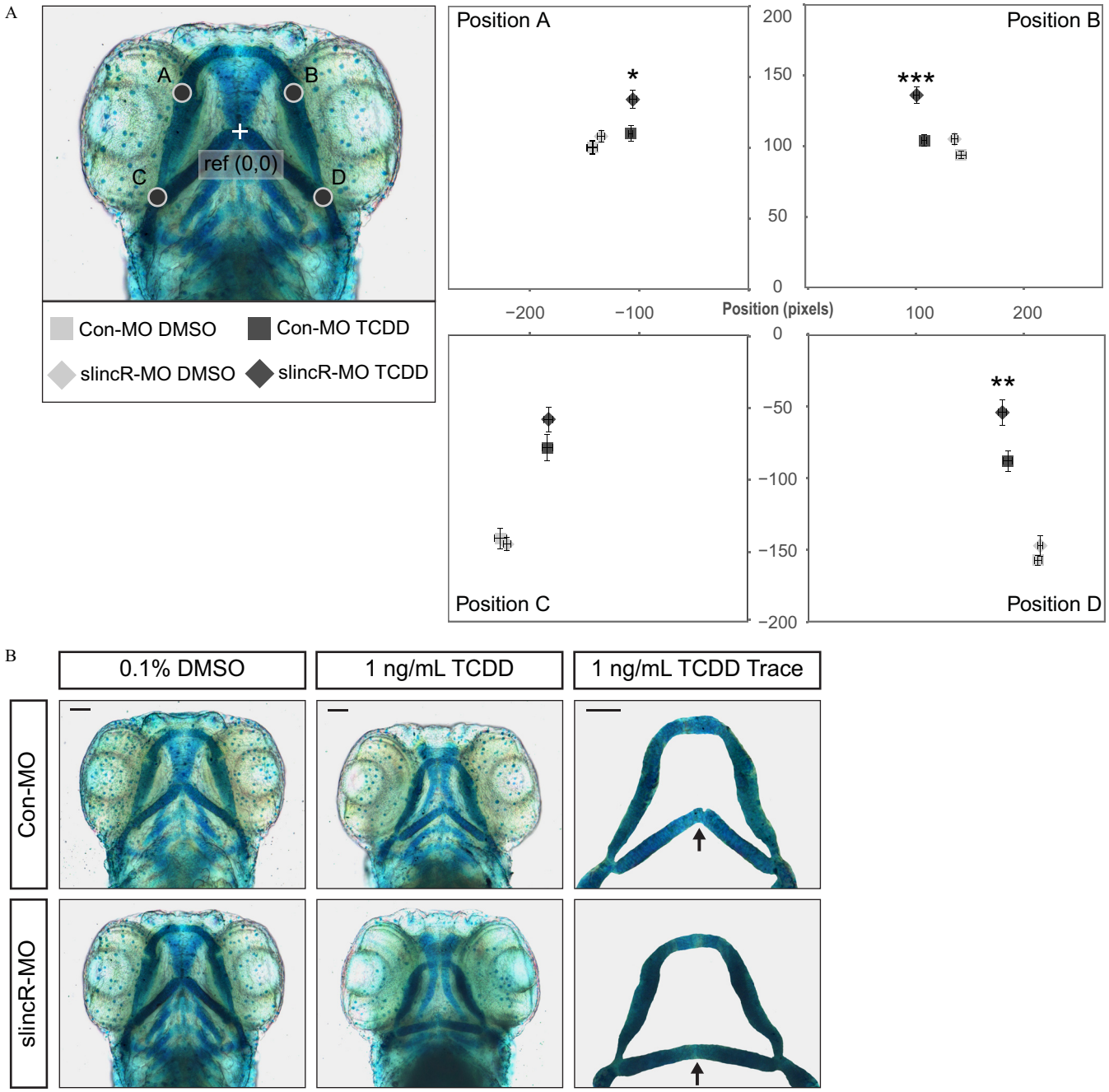

Figure 4. Effect of 1 ng/mL TCDD on the developing jaw after treatment of control and *slincR* morphants. Control (Con-MO) and *slincR* morphants (slincR-MO) were developmentally exposed to 0.1% DMSO or 1 ng/mL TCDD, and the cartilage was stained and measured at 72 hpf. (*A*) A morphometric system was used to measure the position and length of landmark structures in the developing jaw. The position of jaw structures representing junctions between Meckel's and palatoquadrate cartilages (point A and B) and representing junctions between the hyosymplectic and ceratohyal cartilages (point C and D) was measured relative to a reference point as shown. Statistical significance was determined by a modified two-way ANOVA with a Tukey post hoc test. Morphometric values represent mean ± standard error of the mean. ($n = 9$–10 individual 72-hpf zebrafish; $p < 0.05 = *$, $p < 0.01 = **$, $p < 0.001 = ***$). The asterisk (*) indicates statistical significance between slincR-MO and Con-MO samples exposed to TCDD. (*B*) Representative images of the cartilage structures in control and *slincR* morphants treated with DMSO or TCDD. The arrow in the TCDD Trace panel points to the junction between the hyosymplectic and ceratohyal cartilages (point C and D). The bar in the top right corner indicates 100 μM. Note: DMSO, dimethyl sulfoxide; hpf, hours post fertilization; TCDD, 2,3,7,8-tetrachlorodibenzo-*p*-dioxin.

previously used the zebrafish model to identify an *ahr2*-dependent long noncoding RNA, *slincR*, whose expression increased upon exposure to multiple Ahr2 ligands (Garcia et al. 2017). We demonstrated that *slincR* was required for the proper expression of *sox9b* during development and *sox9b* repression in response to TCDD, a strong AHR ligand (Garcia et al. 2017).

PART I: Transcriptional Regulation by slincR

Our data suggested that *slincR* acted in *cis* to repress *sox9b* expression. Biochemical evidence has demonstrated that many lncRNAs act as guides to chromatin-modifying enzymes and/or platforms for protein complexes to regulate the three-dimensional structure of the genome (Quinn and Chang 2016). In the present

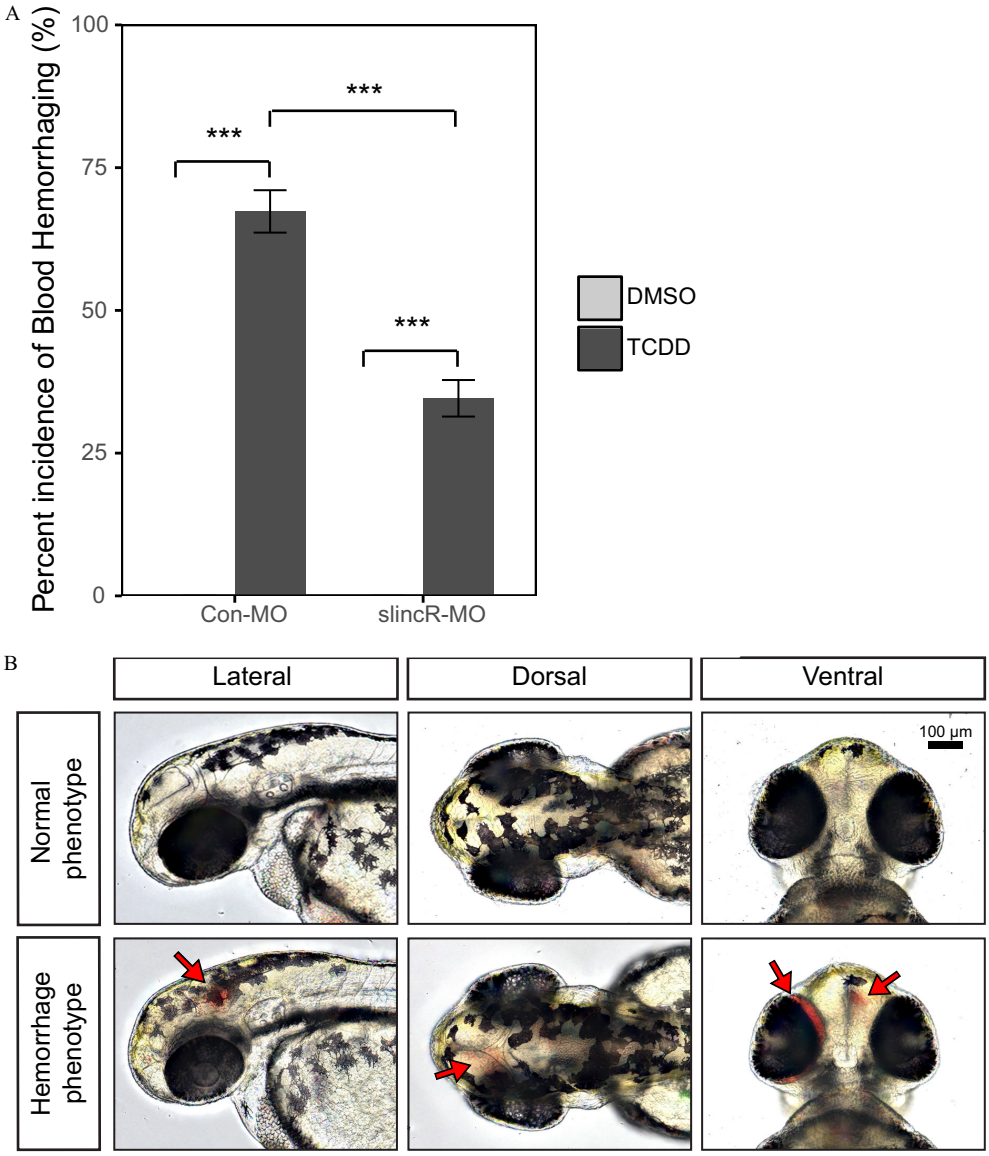

Figure 5. TCDD-induced hemorrhaging in control and *slincR* morphants. Control (Con-MO) and *slincR* morphants (slincR-MO) were developmentally exposed to 0.1% DMSO or 1 ng/mL TCDD, and 48-hpf zebrafish embryos were evaluated for the presence or absence of hemorrhaging. (*A*) The percent incidence of the hemorrhaging phenotype in control and *slincR* morphants exposed to DMSO or TCDD. The DMSO and TCDD samples consisted of 3 and 5 biological replicates, respectively. Each biological replicate contained 10–12 individual 48-hpf zebrafish. All error bars indicate standard error of the mean. Statistical significance was determined using the Type III one-way ANOVA for unbalanced experimental designs from the car package with a Tukey post hoc test ($n = 3$ or 5, $p < 0.001 = ***$). (*B*) Representative images of 48-hpf wild-type zebrafish exposed to DMSO (normal phenotype) or TCDD (hemorrhaging phenotype). The bar in the top right corner indicates 100 µM and arrows point to sites of hemorrhaging. Note: DMSO, dimethyl sulfoxide; hpf, hours post fertilization; TCDD, 2,3,7,8-tetrachlorodibenzo-*p*-dioxin.

study, our data suggest that *slincR* regulates the expression of *sox9b* via enrichment at the 5' UTR of the *sox9b* locus. Further experiments are needed to distinguish whether *slincR* binds directly to the DNA or indirectly via a protein/RNA intermediate. Surprisingly, the DMSO- and TCDD-exposed samples produced similar yields of *slincR* RNA and *sox9b* 5' UTR DNA enrichment, despite the significant increase in *slincR* expression induced upon exposure to TCDD. One possible explanation is that the probe accessibility of the *slincR* transcript is altered due to changes in the interacting molecular partners, which may be condition specific. Additionally, knocking down *sox9b* expression resulted in a significant increase in *slincR* expression. Our previous publication demonstrated that *slincR* was required for the TCDD-induced repression of *sox9b*, had a significant effect on the expression of known *sox9b* target genes, and is expressed in tissues with *sox9b* essential functions (Garcia et al. 2017). These data imply that *sox9b* and *slincR* may share overlapping regulatory networks.

We detected a clear concentration–response relationship between TCDD exposure and the gene expression of *slincR* and *sox9b*. We also evaluated the morphology and behavior of exposed zebrafish in order to correlate the gene expression with the observed toxicity. Although the 0.25, 0.5, and 1.0 ng/mL concentrations of TCDD produced visible malformations in the eye, brain, jaw, snout, and other tissues, only the two highest concentrations of TCDD tested (0.5 and 1.0 ng/mL) were able to both significantly increase *slincR* and significantly decrease *sox9b* expression levels. In response to developmental exposure to 1 ng/mL TCDD, *sox9b* expression is reduced in the eye, brain, otic vesicle, jaw region, and snout region (Garcia et al. 2017). For the 0.25 ng/mL TCDD concentration, the discrepancy

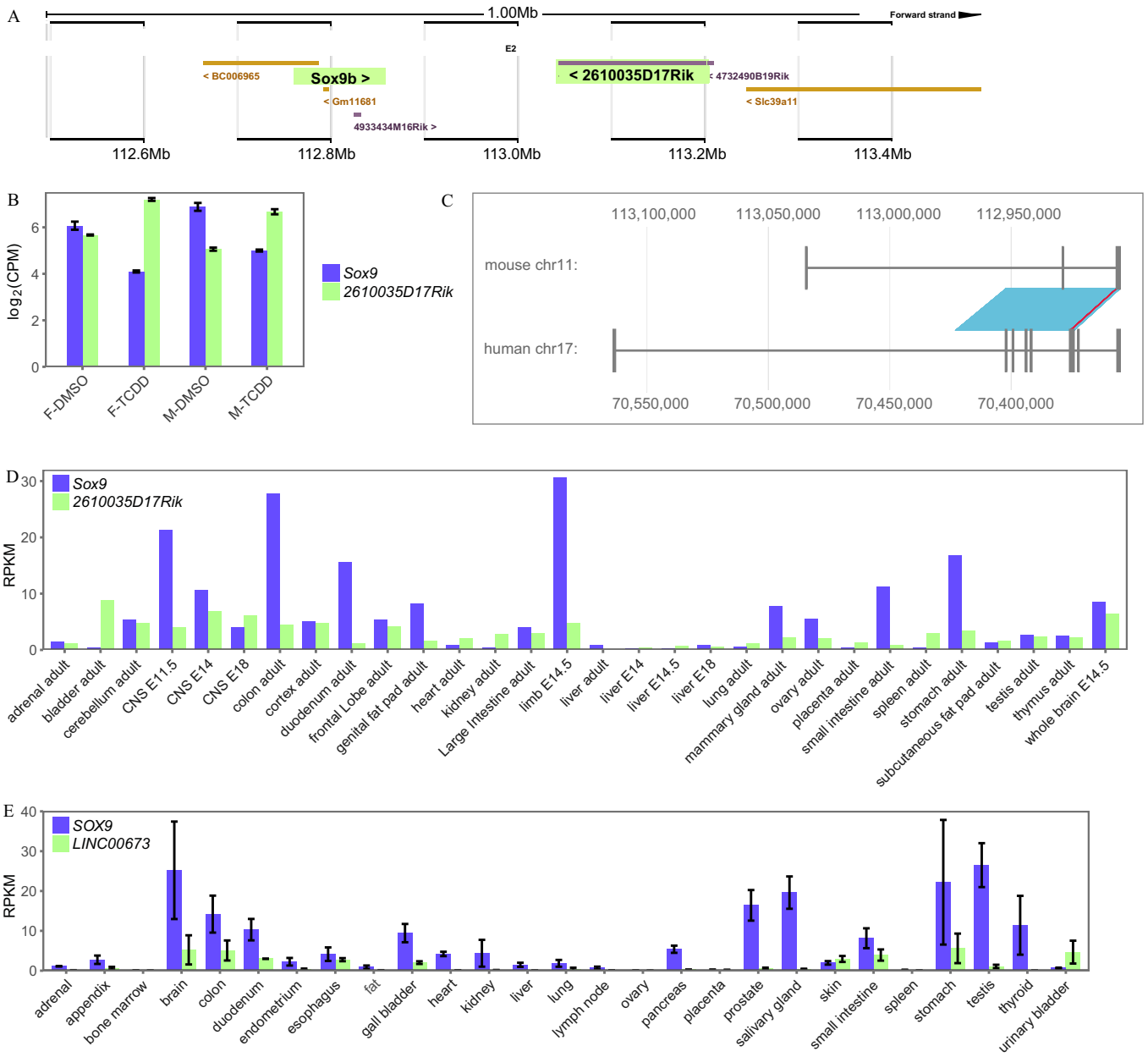

Figure 6. Identification of the potential *slincR* mouse and human orthologs. We identified the potential mouse ortholog of *slincR* (*2610035D17Rik*) based on (*A*) the conserved genomic location and orientation relative to *Sox9* and (*B*) the significant increase in expression in TCDD-exposed mouse urogenital tissue samples from embryonic day 16.5 (F, female and M, male). Each biological sample consisted of RNA from 5–6 pooled mouse urogenital tissue with 3–4 biological replicates per condition. Error bars indicate standard error of the mean. The image from (*A*) was downloaded from the Ensembl mouse genome (GRCm38), and *Sox9* and 2610035D17Rik are highlighted. (*C*) Downloaded and formatted image from the *slncky* Evolution Browser of the mouse (*2610035D17Rik*) and human (*LINC00673*) conserved lncRNA orthologs. To determine the tissue-specific expression of (*D*) mouse- (*2610035D17Rik*) and (*E*) human-conserved (*LINC00673*) lncRNAs relative to *Sox9*/*SOX9*, we downloaded RNA-seq expression data from NCBI BioProjects PRJNA66167 and PRJEB4337, respectively. Error bars indicate standard error of the mean. Note: CPM, counts per million; RPKM, reads per kilobase million.

between the nonsignificant *sox9b* gene expression and significant malformations in the cartilage area may be because the RNA was isolated from a pool of whole embryos, which does not allow for tissue-specific resolution.

PART II: slincR *Contributions to TCDD Toxicity*

SOX9 is required for proper vertebrate development and regulates cell maintenance and specification during adulthood (Barrionuevo et al. 2016; Furuyama et al. 2011; Jo et al. 2014). Overexpression of *SOX9* is associated with liver fibrosis and multiple cancer types (Pritchett et al. 2011). In zebrafish, *sox9b* has a causal role in the Ahr2 toxicity pathway. Antisense knockdown of *sox9b* is sufficient to recapitulate the craniofacial cartilage malformations induced by exposure to TCDD (Xiong et al. 2008). Developmental TCDD-induced repression of *sox9b* decreases both the size and number of chondrocytes to produce malformed craniofacial cartilages (Burns et al. 2015). In addition, *ahr2*-mutant zebrafish also display craniofacial skeletal abnormalities, further supporting the intersection of the AHR and SOX9 regulatory networks (Garcia et al. 2018; Goodale et al. 2012). To understand the functional role of *slincR* in TCDD-induced developmental toxicity, we investigated global transcriptional responses and performed functional enrichment analyses on control and *slincR* morphants

exposed to 1 ng/mL TCDD. Upon exposure to TCDD, an increase in *slincR* expression is required for the functional enrichment of many *sox9b*-regulated processes, including cartilage development, ossification, and bone remodeling, as well as cell adhesion and cell matrix interactions (SOX9 functions reviewed in Jo et al. 2014). We saw evidence that *slincR* knockdown in the presence of TCDD can also alter the structure of craniofacial cartilage. In our morphometric analysis of the cartilage structure, both the control and *slincR* morphants exposed to TCDD exhibited cartilage malformations; however, the *slincR* morphants showed an abnormal junction between hyosymplectic and ceratohyal cartilages in comparison with control morphants. The functional enrichment and morphometric analyses support the hypothesis that, upon TCDD exposure, Ahr2 increases the expression of *slincR*, which in turn represses *sox9b* via enrichment at the 5' UTR, to produce craniofacial cartilage malformations. It is possible that the abnormal cartilage morphology in the *slincR* morphants is due to incomplete *slincR* knockdown and thus incomplete *sox9b* repression (i.e., higher expression of *sox9b*) relative to the levels in the control morphant samples exposed to TCDD. In other words, differing expression levels of *sox9b* may be responsible for the altered cartilage structure, because *sox9b* is a master regulator of cartilage development.

In addition to the AHR-dependent induction of *slincR*, other factors may be acting to repress *sox9b* expression. For example, crosstalk between AHR and Wnt/β-catenin signaling pathways is well established (Schneider et al. 2014; Wincent et al. 2015). In mammalian epithelial stem cell *in vitro* experiments, *SOX9* and *WNT* signaling cooperate in a mutually repressive manner to regulate proliferation, differentiation, and quiescence (Menzel-Severing et al. 2018). In mice, deletion of β-catenin in head mesenchyme provided *in vivo* evidence that suggests β-catenin is essential for proper skeletal linage differentiation by inhibiting mesenchymal osteoblastic cells from entering the chondrocyte linage (Hill et al. 2005). Gene expression measurements in the β-catenin mutant displayed a significant increase in expression of *Sox9* and its upstream regulator *Runx2*, which argues that β-catenin is not directly regulating *Sox9*. In zebrafish, several publications have supported the hypothesis that xenobiotic activation of the AHR leads to a disruption in Wnt/β-catenin signaling, and that this disruption in Wnt signaling has a causal role in AHR-mediated toxicities (Mathew et al. 2008; Wincent et al. 2015). Using the zebrafish caudal fin regeneration model, we have previously shown that TCDD-induced AHR activation blocks the tissue regeneration process via activation of the Wnt/β-catenin signaling pathway, leading to improper formation of the wound epithelium and blastema (Mathew et al. 2008). The TCDD-induced block in caudal fin regeneration is prevented by antisense knockdown of a Wnt coreceptor (*lrp6*) that induces β-catenin signaling. In addition, exposure to a pharmacological agent (6-bromoindirubin-3′-oxime) that overactivates the Wnt signaling pathway phenocopied the TCDD-induced block in fin regeneration. In response to AHR activation, it is likely that genes involved in multiple signaling pathways are disrupted and acting in concert to repress expression of *sox9b* and/or inhibit normal cartilage development.

The AHR regulates vasculature remodeling of the developing embryo, and dysregulation can lead to abnormal development of vasculature structures (Lahvis et al. 2000; Walisser et al. 2004). Developmental exposure to TCDD or PAHs can produce blood circulation defects and *cyp1a1* expression in the vasculature (Andreasen et al. 2002; Chlebowski et al. 2017; Henry et al. 1997). Our transcriptome profiling and functional enrichment analyses suggest *slincR* expression regulates processes involved in angiogenesis, vascular smooth-muscle cell proliferation, blood vessel endothelial cell migration, blood coagulation, and blood vessel morphogenesis.

Upon exposure to a strong Ahr2 ligand, a toxicity phenotype that occurs early in zebrafish development is disruption of blood cell development and hemorrhaging (Belair et al. 2001; Henry et al. 1997). To elucidate the phenotypic impact of *slincR* expression on TCDD-induced hemorrhaging, we developmentally exposed control and *slincR* morphants to TCDD and recorded the presence or absence of hemorrhaging. In concordance with the RNA-seq data, we demonstrated that upon TCDD exposure, preventing the induction of *slincR* can prevent a significant percentage of zebrafish from displaying the hemorrhaging phenotype; however, knocking down *slincR* did not result in the complete absence of the hemorrhaging phenotype. Although this discrepancy could be due to the incomplete knockdown of *slincR*, it is also possible that the activation of the AHR results in the dysregulation of multiple regulatory networks that are required for normal angiogenesis and vascular development. Our data suggest *ahr2*-dependent expression of *slincR* plays a causal role in TCDD-induced hemorrhaging. Additional experiments are required to understand how *slincR* expression regulates processes such as angiogenesis and vasculature development at the gene-network, cellular, and tissue levels.

PART III: Investigation of PAHs that Increase slincR *Expression*

The AHR is ligand-activated by numerous PAHs, which pose a major concern due to their potential toxic effects on ecosystems and human health (Chlebowski et al. 2017; Geier et al. 2018; Perera 1997). For example, exposure of pregnant women to high levels of air pollution, which is a complex heterogeneous mixture containing numerous PAHs, has been associated with an increase in the risk of impaired neural development and congenital heart defects in their children (Brook et al. 2004; Edwards et al. 2010). To screen for environmentally relevant PAHs that upregulate *slincR* expression and activate the AHR signaling pathway, we mined a 16 PAH RNA-seq dataset from 48-hpf whole zebrafish embryos generated by Dr. M. Geier from the Tanguay lab. We identified six PAHs that significantly up-regulate *slincR* expression, including benzo[*k*]fluoranthene, dibenzo[*a*,*h*]pyrene, and dibenzo[*a*,*i*]pyrene from the U.S. Environmental Protection Agency's priority PAH list. Our screen also identified three PAHs (retene, dibenzo[*a*,*h*]pyrene, and dibenzo[*a*,*i*]pyrene) that cause a significant increase in *slincR* expression and were recently shown to induce *cyp1a1* vasculature expression (Geier et al. 2018). The Geier study also reported that fluoranthene and 9-methylanthracene induced *cyp1a1* expression in the vasculature; however, our data did not show a significant increase in *slincR* expression for these two PAHs, emphasizing the ligand-specific transcriptional responses of AHR activation (Geier et al. 2018).

None of the PAHs screened resulted in a significant decrease in *sox9b* expression even though benzo[*k*]fluoranthene and benzo[*j*]fluoranthene were able to produce larger $\log_2$(fold change) increases (4.0 and 3.9) in *slincR* expression than did TCDD exposure (3.1). LncRNAs have a more restricted tissue-specific expression pattern in comparison with mRNAs (Fatica and Bozzoni 2014). Thus, it is possible that *slincR* induction was localized to tissue where *sox9b* is not highly expressed. We previously showed that exposure to TCDD increased *slincR* expression in the otic vesicle and jaw or snout regions (Garcia et al. 2017). It is also possible that *slincR* regulates additional genes, beyond *sox9b*. Future experiments will identify the tissues in which *slincR* expression is increased upon exposure to select PAHs. Elucidating the transcriptional responses and target organs of ligand-specific AHR activation is a key process required to begin to classify and predict how chemicals, like PAHs, produce toxic responses. The developmental toxicity and functional enrichment

analyses of the 16 PAHs screened will be addressed in a forthcoming study from the Tanguay laboratory.

Our current study includes several limitations. For example, we used morpholinos, which are a transient method of knocking down gene expression. Another limitation of our study is that we were unable to maintain adequate *slincR* repression at 72 hpf, which prevents us from fully understanding the functional impact of *slincR* expression on TCDD-induced toxicity phenotypes that occur later in development. In future studies, we will use a CRISPR/Cas9-generated *slincR* knockout line to determine the phenotypic impact of *slincR* expression on later developmental stages. Additionally, our RNA sequencing analysis resulted in a dramatic decrease in the number of significant genes in response to TCDD exposure in the *slincR* morphants, in comparison with control morphants. One notable limitation of RNA sequencing is the inability to distinguish direct and indirect changes in gene expression; therefore, we are unable to determine if the difference in gene expression is because of the direct regulation of *slincR* on *sox9b* and additional target genes or if the difference is because of indirect regulation downstream of *slincR* target genes. Future studies will identify the genome-wide binding sites of *slincR* using CHART-sequencing, which has previously shown that lncRNAs can bind hundreds of regions throughout the genome to regulate transcription (West et al. 2014).

Conclusion

We further elucidated the mechanism of TCDD-induced repression of *sox9b* in the developing zebrafish by showing that *slincR* is enriched at the 5' UTR of the *sox9b* locus to repress transcription. We used transcriptome profiling and functional enrichment analyses to demonstrate that *ahr2*-dependent expression of *slincR* is involved in processes such as angiogenesis and cartilage and vasculature development. Our data suggest that *slincR* expression may play a causal role in the TCDD-induced hemorrhaging phenotype, can regulate cartilage development, and is up-regulated by multiple environmentally relevant PAHs. We identified potential mouse and human orthologs of *slincR* in support of the human health relevance of the zebrafish model. In summary, these data enhance our mechanistic understanding of how AHR activation by environmental pollutants can lead to adverse health effects.

Acknowledgments

This research was partially supported by NIH grants P42 ES016465, R21 ES025421, T32 ES07060, F31 ES026518, and P30 ES000210. The content is solely the responsibility of the authors and does not necessarily represent the official views of the NIH. We would also like to thank the agents of Sinnhuber Aquatic Research Laboratory (SARL), especially C. Barton and G. Gonnerman, for all their help regarding fish husbandry. Finally, we thank the generosity of Dr. R. Peterson and Dr. M. Geier for allowing us to mine their unpublished RNA sequencing datasets, which greatly enhanced the quality of this study.

References

Akiyama H, Chaboissier MC, Martin JF, Schedl A, de Crombrugghe B. 2002. The transcription factor Sox9 has essential roles in successive steps of the chondrocyte differentiation pathway and is required for expression of Sox5 and Sox6. Genes Dev 16(21):2813–2828, PMID: 12414734, https://doi.org/10.1101/gad.1017802.

Anders S, McCarthy DJ, Chen Y, Okoniewski M, Smyth GK, Huber W, et al. 2013. Count-based differential expression analysis of RNA sequencing data using R and Bioconductor. Nat Protoc 8(9):1765–1786, PMID: 23975260, https://doi.org/10.1038/nprot.2013.099.

Anders S, Pyl PT, Huber W. 2015. HTSeq–a Python framework to work with high-throughput sequencing data. Bioinformatics 31(2):166–169, PMID: 25260700, https://doi.org/10.1093/bioinformatics/btu638.

Andreasen EA, Spitsbergen JM, Tanguay RL, Stegeman JJ, Heideman W, Peterson RE. 2002. Tissue-specific expression of AHR2, ARNT2, and CYP1A in zebrafish embryos and larvae: effects of developmental stage and 2,3,7,8-tetrachlorodibenzo-p-dioxin exposure. Toxicol Sci 68(2):403–419, PMID: 12151636, https://doi.org/10.1093/toxsci/68.2.403.

Andrews S. 2015. *FastQC: A Quality Control Tool for High Throughput Sequence Data. Version 0.11.3.* Cambridge, UK: Babraham Bioinformatics. https://www.bioinformatics.babraham.ac.uk/projects/fastqc/.

Antkiewicz DS, Peterson RE, Heideman W. 2006. Blocking expression of AHR2 and ARNT1 in zebrafish larvae protects against cardiac toxicity of 2,3,7,8-tetrachlorodibenzo-p-dioxin. Toxicol Sci 94(1):175–182, PMID: 16936225, https://doi.org/10.1093/toxsci/kfl093.

Barrionuevo FJ, Hurtado A, Kim G-J, Real FM, Bakkali M, Kopp JL, et al. 2016. Sox9 and Sox8 protect the adult testis from male-to-female genetic reprogramming and complete degeneration. Elife 5:e15635, PMID: 27328324, https://doi.org/10.7554/eLife.15635.

Barton CL, Johnson EW, Tanguay RL. 2016. Facility design and health management program at the Sinnhuber Aquatic Research Laboratory. Zebrafish 13(Suppl 1):S39–S43, PMID: 26981844, https://doi.org/10.1089/zeb.2015.1232.

Beischlag TV, Luis Morales J, Hollingshead BD, Perdew GH. 2008. The aryl hydrocarbon receptor complex and the control of gene expression. Crit Rev Eukaryot Gene Expr 18(3):207–250, PMID: 18540824, https://doi.org/10.1615/CritRevEukarGeneExpr.v18.i3.20.

Belair CD, Peterson RE, Heideman W. 2001. Disruption of erythropoiesis by dioxin in the zebrafish. Dev Dyn 222(4):581–594, PMID: 11748828, https://doi.org/10.1002/dvdy.1213.

Bogdanović O, Fernández-Miñán A, Tena JJ, de la Calle-Mustienes E, Gómez-Skarmeta JL. 2013. The developmental epigenomics toolbox: ChIP-seq and MethylCap-seq profiling of early zebrafish embryos. Methods 62(3):207–215, PMID: 23624103, https://doi.org/10.1016/j.ymeth.2013.04.011.

Boström CE, Gerde P, Hanberg A, Jernström B, Johansson C, Kyrklund T, et al. 2002. Cancer risk assessment, indicators, and guidelines for polycyclic aromatic hydrocarbons in the ambient air. Environ Health Perspect 110(suppl 3):451–488, https://doi.org/10.1289/ehp.110-1241197.

Branam AM, Davis NM, Moore RW, Schneider AJ, Vezina CM, Peterson RE. 2013. TCDD inhibition of canonical Wnt signaling disrupts prostatic bud formation in mouse urogenital sinus. Toxicol Sci 133(1):42–53, PMID: 23429912, https://doi.org/10.1093/toxsci/kft027.

Brook RD, Franklin B, Cascio W, Hong Y, Howard G, Lipsett M, et al. 2004. Air pollution and cardiovascular disease: a statement for healthcare professionals from the Expert Panel on Population and Prevention Science of the American Heart Association. Circulation 109(21):2655–2671, PMID: 15173049, https://doi.org/10.1161/01.CIR.0000128587.30041.C8.

Burns FR, Peterson RE, Heideman W. 2015. Dioxin disrupts cranial cartilage and dermal bone development in zebrafish larvae. Aquat Toxicol 164:52–60, PMID: 25914093, https://doi.org/10.1016/j.aquatox.2015.04.005.

Carney SA, Prasch AL, Heideman W, Peterson RE. 2006. Understanding dioxin developmental toxicity using the zebrafish model. Birth Defects Res Part A Clin Mol Teratol 76(1):7–18, PMID: 16333842, https://doi.org/10.1002/bdra.20216.

Chen Y, Lun AT, Smyth GK. 2016. From reads to genes to pathways: differential expression analysis of RNA-seq experiments using Rsubread and the edgeR quasi-likelihood pipeline. F1000Res 5:1438, PMID: 27508061, https://doi.org/10.12688/f1000research.8987.2.

Chen Y, Lun ATL, Smyth GK. 2014. Differential expression analysis of complex RNA-seq experiments using edgeR. In: *Statistical Analysis of Next Generation Sequencing Data*, (Datta S, Nettleton D, eds). Cham, Switzerland: Springer International Publishing, 51–74.

Chen J, Shishkin AA, Zhu X, Kadri S, Maza I, Guttman M, et al. 2016. Evolutionary analysis across mammals reveals distinct classes of long non-coding RNAs. Genome Biol 17:19, PMID: 26838501, https://doi.org/10.1186/s13059-016-0880-9.

Chlebowski AC, Garcia GR, La Du JK, Bisson WH, Truong L, Massey Simonich SL, et al. 2017. Mechanistic investigations into the developmental toxicity of nitrated and heterocyclic PAHs. Toxicol Sci 157(1):246–259, PMID: 28186253, https://doi.org/10.1093/toxsci/kfx035.

Couture LA, Abbott BD, Birnbaum LS. 1990. A critical review of the developmental toxicity and teratogenicity of 2,3,7,8-tetrachlorodibenzo-p-dioxin: recent advances toward understanding the mechanism. Teratology 42(6):619–627, PMID: 2087682, https://doi.org/10.1002/tera.1420420606.

Dejmek J, Solanský I, Benes I, Lenícek J, Srám RJ. 2000. The impact of polycyclic aromatic hydrocarbons and fine particles on pregnancy outcome. Environ Health Perspect 108(12):1159–1164, PMID: 11133396, https://doi.org/10.1289/ehp.001081159.

Denison MS, Nagy SR. 2003. Activation of the aryl hydrocarbon receptor by structurally diverse exogenous and endogenous chemicals. Annu Rev Pharmacol Toxicol 43:309–334, PMID: 12540743, https://doi.org/10.1146/annurev.pharmtox.43.100901.135828.

DeVito MJ, Birnbaum LS. 1995. The importance of pharmacokinetics in determining the relative potency of 2,3,7,8-tetrachlorodibenzo-p-dioxin and 2,3,7,8-tetrachlorodibenzofuran. Fundam Appl Toxicol 24(1):145–148, PMID: 7713338.

Durinck S, Moreau Y, Kasprzyk A, Davis S, De Moor B, Brazma A, et al. 2005. BioMart and Bioconductor: a powerful link between biological databases and microarray data analysis. Bioinformatics 21(16):3439–3440, PMID: 16082012, https://doi.org/10.1093/bioinformatics/bti525.

Durinck S, Spellman PT, Birney E, Huber W. 2009. Mapping identifiers for the integration of genomic datasets with the R/Bioconductor package biomaRt. Nat Protoc 4(8):1184–1191, PMID: 19617889, https://doi.org/10.1038/nprot.2009.97.

Edwards SC, Jedrychowski W, Butscher M, Camann D, Kieltyka A, Mroz E, et al. 2010. Prenatal exposure to airborne polycyclic aromatic hydrocarbons and children's intelligence at 5 years of age in a prospective cohort study in Poland. Environ Health Perspect 118(9):1326–1331, PMID: 20406721, https://doi.org/10.1289/ehp.0901070.

Esser C, Rannug A. 2015. The aryl hydrocarbon receptor in barrier organ physiology, immunology, and toxicology. Pharmacol Rev 67(2):259–279, PMID: 25657351, https://doi.org/10.1124/pr.114.009001.

Fagerberg L, Hallström BM, Oksvold P, Kampf C, Djureinovic D, Odeberg J, et al. 2014. Analysis of the human tissue-specific expression by genome-wide integration of transcriptomics and antibody-based proteomics. Mol Cell Proteomics 13(2):397–406, PMID: 24309898, https://doi.org/10.1074/mcp.M113.035600.

Fatica A, Bozzoni I. 2014. Long non-coding RNAs: new players in cell differentiation and development. Nat Rev Genet 15(1):7–21, PMID: 24296535, https://doi.org/10.1038/nrg3606.

Fernandez-Salguero P, Pineau T, Hilbert DM, McPhail T, Lee SS, Kimura S, et al. 1995. Immune system impairment and hepatic fibrosis in mice lacking the dioxin-binding Ah receptor. Science 268(5211):722–726, PMID: 7732381, https://doi.org/10.1126/science.7732381.

Fox J, Weisberg S. 2011. *An R Companion to Applied Regression*. 2nd ed. Thousand Oaks, CA: Sage.

Furuyama K, Kawaguchi Y, Akiyama H, Horiguchi M, Kodama S, Kuhara T, et al. 2011. Continuous cell supply from a Sox9-expressing progenitor zone in adult liver, exocrine pancreas and intestine. Nat Genet 43:34–41, PMID: 21113154, https://doi.org/10.1038/ng.722.

Garcia GR, Bugel SM, Truong L, Spagnoli S, Tanguay RL. 2018. AHR2 required for normal behavioral responses and proper development of the skeletal and reproductive systems in zebrafish. PLoS One 13(3):e0193484, PMID: 29494622, https://doi.org/10.1371/journal.pone.0193484.

Garcia GR, Goodale BC, Wiley MW, La Du JK, Hendrix DA, Tanguay RL. 2017. In vivo characterization of an AHR-dependent long noncoding RNA required for proper Sox9b expression. Mol Pharmacol 91(6):609–619, PMID: 28385905, https://doi.org/10.1124/mol.117.108233.

Garcia GR, Noyes PD, Tanguay RL. 2016. Advancements in zebrafish applications for 21st century toxicology. Pharmacol Ther 161:11–21, PMID: 27016469, https://doi.org/10.1016/j.pharmthera.2016.03.009.

Geier MC, Chlebowski AC, Truong L, Massey Simonich SL, Anderson KA, Tanguay RL. 2018. Comparative developmental toxicity of a comprehensive suite of polycyclic aromatic hydrocarbons. Arch Toxicol 92(2):571–586, PMID: 29094189, https://doi.org/10.1007/s00204-017-2068-9.

Goodale BC, La Du JK, Bisson WH, Janszen DB, Waters KM, Tanguay RL. 2012. AHR2 mutant reveals functional diversity of aryl hydrocarbon receptors in zebrafish. PLoS One 7(1):e29346, PMID: 22242167, https://doi.org/10.1371/journal.pone.0029346.

Goodale BC, La Du J, Tilton SC, Sullivan CM, Bisson WH, Waters KM, et al. 2015. Ligand-specific transcriptional mechanisms underlie aryl hydrocarbon receptor-mediated developmental toxicity of oxygenated PAHs. Toxicol Sci 147(2):397–411, PMID: 26141390, https://doi.org/10.1093/toxsci/kfv139.

Gu Z, Eils R, Schlesner M. 2016. Complex heatmaps reveal patterns and correlations in multidimensional genomic data. Bioinformatics 32(18):2847–2849, PMID: 27207943, https://doi.org/10.1093/bioinformatics/btw313.

Gutschner T, Diederichs S. 2012. The hallmarks of cancer: a long non-coding RNA point of view. RNA Biol 9(6):703–719, PMID: 22664915, https://doi.org/10.4161/rna.20481.

Haggard DE, Noyes PD, Waters KM, Tanguay RL. 2016. Phenotypically anchored transcriptome profiling of developmental exposure to the antimicrobial agent, triclosan, reveals hepatotoxicity in embryonic zebrafish. Toxicol Appl Pharmacol 308:32–45, PMID: 27538710, https://doi.org/10.1016/j.taap.2016.08.013.

Hahn ME, Karchner SI, Merson RR. 2017. Diversity as opportunity: insights from 600 million years of AHR evolution. Curr Opin Toxicol 2:58–71, PMID: 28286876, https://doi.org/10.1016/j.cotox.2017.02.003.

Henry TR, Spitsbergen JM, Hornung MW, Abnet CC, Peterson RE. 1997. Early life stage toxicity of 2,3,7,8-tetrachlorodibenzo-p-dioxin in zebrafish (Danio rerio). Toxicol Appl Pharmacol 142(1):56–68, PMID: 9007034, https://doi.org/10.1006/taap.1996.8024.

Herberich E, Sikorski J, Hothorn T. 2010. A robust procedure for comparing multiple means under heteroscedasticity in unbalanced designs. PLOS One 5(3):e9788, PMID: 20360960, https://doi.org/10.1371/journal.pone.0009788.

Hill TP, Später D, Taketo MM, Birchmeier W, Hartmann C. 2005. Canonical Wnt/beta-catenin signaling prevents osteoblasts from differentiating into chondrocytes. Dev Cell 8(5):727–738, PMID: 15866163, https://doi.org/10.1016/j.devcel.2005.02.013.

Hofsteen P, Plavicki J, Johnson SD, Peterson RE, Heideman W. 2013. Sox9b is required for epicardium formation and plays a role in TCDD-induced heart malformation in zebrafish. Mol Pharmacol 84(3):353–360, PMID: 23775563, https://doi.org/10.1124/mol.113.086413.

Hothorn T, Bretz F, Westfall P. 2008. Simultaneous inference in general parametric models. Biom J 50(3):346–363, PMID: 18481363, https://doi.org/10.1002/bimj.200810425.

Howe K, Clark MD, Torroja CF, Torrance J, Berthelot C, Muffato M, et al. 2013. The zebrafish reference genome sequence and its relationship to the human genome. Nature 496(7446):498–503, PMID: 23594743, https://doi.org/10.1038/nature12111.

Huang S, Shui X, He Y, Xue Y, Li J, Li G, et al. 2015. AhR expression and polymorphisms are associated with risk of coronary arterial disease in Chinese population. Sci Rep 5:8022, PMID: 25620626, https://doi.org/10.1038/srep08022.

Huber W, Carey VJ, Gentleman R, Anders S, Carlson M, Carvalho BS, et al. 2015. Orchestrating high-throughput genomic analysis with Bioconductor. Nat Methods 12(2):115–121, PMID: 25633503, https://doi.org/10.1038/nmeth.3252.

Jiang H, Lei R, Ding SW, Zhu S. 2014. Skewer: a fast and accurate adapter trimmer for next-generation sequencing paired-end reads. BMC Bioinformatics 15:182, PMID: 24925680, https://doi.org/10.1186/1471-2105-15-182.

Jo A, Denduluri S, Zhang B, Wang Z, Yin L, Yan Z, et al. 2014. The versatile functions of Sox9 in development, stem cells, and human diseases. Genes Dis 1(2):149–161, PMID: 25685828, https://doi.org/10.1016/j.gendis.2014.09.004.

Kim D, Pertea G, Trapnell C, Pimentel H, Kelley R, Salzberg SL. 2013. TopHat2: accurate alignment of transcriptomes in the presence of insertions, deletions and gene fusions. Genome Biol 14(4):R36, PMID: 23618408, https://doi.org/10.1186/gb-2013-14-4-r36.

Knecht AL, Truong L, Simonich MT, Tanguay RL. 2017. Developmental benzo[a]pyrene (B[a]P) exposure impacts larval behavior and impairs adult learning in zebrafish. Neurotoxicol Teratol 59:27–34, PMID: 27989697, https://doi.org/10.1016/j.ntt.2016.10.006.

Lahvis GP, Lindell SL, Thomas RS, McCuskey RS, Murphy C, Glover E, et al. 2000. Portosystemic shunting and persistent fetal vascular structures in aryl hydrocarbon receptor-deficient mice. Proc Natl Acad Sci U S A 97(19):10442–10447, PMID: 10973493, https://doi.org/10.1073/pnas.190256997.

Langmead B, Salzberg SL. 2012. Fast gapped-read alignment with Bowtie 2. Nat Methods 9(4):357–359, PMID: 22388286, https://doi.org/10.1038/nmeth.1923.

Langmead B, Trapnell C, Pop M, Salzberg SL. 2009. Ultrafast and memory-efficient alignment of short DNA sequences to the human genome. Genome Biol 10(3):R25, PMID: 19261174, https://doi.org/10.1186/gb-2009-10-3-r25.

Li L, Chang HY. 2014. Physiological roles of long noncoding RNAs: insight from knockout mice. Trends Cell Biol 24(10):594–602, PMID: 25022466, https://doi.org/10.1016/j.tcb.2014.06.003.

Li H, Handsaker B, Wysoker A, Fennell T, Ruan J, Homer N, et al. 2009. The sequence alignment/map format and SAMtools. Bioinformatics 25(16):2078–2079, PMID: 19505943, https://doi.org/10.1093/bioinformatics/btp352.

Lin TM, Rasmussen NT, Moore RW, Albrecht RM, Peterson RE. 2003. Region-specific inhibition of prostatic epithelial bud formation in the urogenital sinus of C57BL/6 mice exposed in utero to 2,3,7,8-tetrachlorodibenzo-p-dioxin. Toxicol Sci 76(1):171–181, PMID: 12944588, https://doi.org/10.1093/toxsci/kfg218.

Livak KJ, Schmittgen TD. 2001. Analysis of relative gene expression data using real-time quantitative PCR and the 2(-delta delta C(T)) method. Methods 25(4):402–408, PMID: 11846609, https://doi.org/10.1006/meth.2001.1262.

Love MI, Anders S, Kim V, Huber W. 2016. RNA-seq workflow: gene-level exploratory analysis and differential expression. [version 2; referees: 2 approved]. F1000Res 4:1070, https://doi.org/10.12688/f1000r.esearch.7035.2.

Lun AT, Chen Y, Smyth GK. 2016. It's DE-licious: a recipe for differential expression analyses of RNA-seq experiments using quasi-likelihood methods in edgeR. Methods Mol Biol 1418:391–416, PMID: 27008025, https://doi.org/10.1007/978-1-4939-3578-9_19.

Mandrell D, Truong L, Jephson C, Sarker MR, Moore A, Lang C, et al. 2012. Automated zebrafish chorion removal and single embryo placement: optimizing throughput of zebrafish developmental toxicity screens. J Lab Autom 17(1):66–74, PMID: 22357610, https://doi.org/10.1177/2211068211432197.

Mathew LK, Sengupta SS, Ladu J, Andreasen EA, Tanguay RL. 2008. Crosstalk between AHR and Wnt signaling through R-spondin1 impairs tissue regeneration in zebrafish. FASEB J 22(8):3087–3096, PMID: 18495758, https://doi.org/10.1096/fj.08-109009.

McCarthy DJ, Chen Y, Smyth GK. 2012. Differential expression analysis of multifactor RNA-seq experiments with respect to biological variation. Nucleic Acids Res 40(10):4288–4297, PMID: 22287627, https://doi.org/10.1093/nar/gks042.
Menzel-Severing J, Zenkel M, Polisetti N, Sock E, Wegner M, Kruse FE, et al. 2018. Transcription factor profiling identifies Sox9 as regulator of proliferation and differentiation in corneal epithelial stem/progenitor cells. Sci Rep 8(1):10268, PMID: 29980721, https://doi.org/10.1038/s41598-018-28596-3.
Murray IA, Patterson AD, Perdew GH. 2014. Aryl hydrocarbon receptor ligands in cancer: friend and foe. Nat Rev Cancer 14(12):801–814, PMID: 25568920, https://doi.org/10.1038/nrc3846.
Nakagawa S. 2016. Lessons from reverse-genetic studies of lncRNAs. Biochim Biophys Acta 1859(1):177–183, PMID: 26117798, https://doi.org/10.1016/j.bbagrm.2015.06.011.
National Research Council. 2007. *Toxicity Testing in the 21st Century: A Vision and a Strategy*. Washington, DC: The National Academies Press.
Noyes PD, Garcia GR, Tanguay RL. 2016. Zebrafish as an in vivo model for sustainable chemical design. Green Chem 18(24):6410–6430, PMID: 28461781, https://doi.org/10.1039/C6GC02061E.
Opitz CA, Litzenburger UM, Sahm F, Ott M, Tritschler I, Trump S, et al. 2011. An endogenous tumour-promoting ligand of the human aryl hydrocarbon receptor. Nature 478(7368):197–203, PMID: 21976023, https://doi.org/10.1038/nature10491.
Perera FP. 1997. Environment and cancer: who are susceptible? Science 278(5340):1068–1073, PMID: 9353182, https://doi.org/10.1126/science.278.5340.1068.
Perera F, Tang D, Whyatt R, Lederman SA, Jedrychowski W. 2005. DNA damage from polycyclic aromatic hydrocarbons measured by benzo[a]pyrene-DNA adducts in mothers and newborns from northern Manhattan, the World Trade Center area, Poland, and China. Cancer Epidemiol Biomarkers Prev 14(3):709–714, PMID: 15767354, https://doi.org/10.1158/1055-9965.EPI-04-0457.
Pritchett J, Athwal V, Roberts N, Hanley NA, Hanley KP. 2011. Understanding the role of SOX9 in acquired diseases: lessons from development. Trends Mol Med 17(3):166–174, PMID: 21237710, https://doi.org/10.1016/j.molmed.2010.12.001.
Quinn JJ, Chang HY. 2016. Unique features of long non-coding RNA biogenesis and function. Nat Rev Genet 17(1):47–62, PMID: 26666209, https://doi.org/10.1038/nrg.2015.10.
Robinson MD, McCarthy DJ, Smyth GK. 2010. edgeR: a Bioconductor package for differential expression analysis of digital gene expression data. Bioinformatics 26(1):139–140, PMID: 19910308, https://doi.org/10.1093/bioinformatics/btp616.
Robinson MD, Oshlack A. 2010. A scaling normalization method for differential expression analysis of RNA-seq data. Genome Biol 11(3):R25, PMID: 20196867, https://doi.org/10.1186/gb-2010-11-3-r25.
Robinson MD, Smyth GK. 2007. Moderated statistical tests for assessing differences in tag abundance. Bioinformatics 23(21):2881–2887, PMID: 17881408, https://doi.org/10.1093/bioinformatics/btm453.
Robinson MD, Smyth GK. 2008. Small-sample estimation of negative binomial dispersion, with applications to sage data. Biostatistics 9(2):321–332, PMID: 17728317, https://doi.org/10.1093/biostatistics/kxm030.
Schneider AJ, Branam AM, Peterson RE. 2014. Intersection of AHR and Wnt signaling in development, health, and disease. Int J Mol Sci 15(10):17852–17885, PMID: 25286307, https://doi.org/10.3390/ijms151017852.
Shen H, Huang Y, Wang R, Zhu D, Li W, Shen G, et al. 2013. Global atmospheric emissions of polycyclic aromatic hydrocarbons from 1960 to 2008 and future predictions. Environ Sci Technol 47(12):6415–6424, PMID: 23659377, https://doi.org/10.1021/es400857z.
Simon MD. 2013. Capture hybridization analysis of RNA targets (CHART). Curr Protoc Mol Biol, PMID: 23288463, https://doi.org/10.1002/0471142727.mb2125s101.
Tang WY, Levin L, Talaska G, Cheung YY, Herbstman J, Tang D, et al. 2012. Maternal exposure to polycyclic aromatic hydrocarbons and 5'-CpG methylation of interferon-γ in cord white blood cells. Environ Health Perspect 120(8):1195–1200, PMID: 22562770, https://doi.org/10.1289/ehp.1103744.
Tanguay RL, Abnet CC, Heideman W, Peterson RE. 1999. Cloning and characterization of the zebrafish (Danio rerio) aryl hydrocarbon receptor. Biochim Biophys Acta 1444(1):35–48, PMID: 9931422, https://doi.org/10.1016/S0167-4781(98)00252-8.
Truong L, Bugel SM, Chlebowski A, Usenko CY, Simonich MT, Simonich SL, et al. 2016. Optimizing multi-dimensional high throughput screening using zebrafish. Reprod Toxicol 65:139–147, PMID: 27453428, https://doi.org/10.1016/j.reprotox.2016.05.015.
Truong L, Reif DM, St Mary L, Geier MC, Truong HD, Tanguay RL. 2014. Multidimensional in vivo hazard assessment using zebrafish. Toxicol Sci 137(1):212–233, PMID: 24136191, https://doi.org/10.1093/toxsci/kft235.
Vezina CM, Lin TM, Peterson RE. 2009. AHR signaling in prostate growth, morphogenesis, and disease. Biochem Pharmacol 77(4):566–576, PMID: 18977204, https://doi.org/10.1016/j.bcp.2008.09.039.
Walisser JA, Bunger MK, Glover E, Bradfield CA. 2004. Gestational exposure of Ahr and Arnt hypomorphs to dioxin rescues vascular development. Proc Natl Acad Sci USA 101(47):16677–16682, PMID: 15545609, https://doi.org/10.1073/pnas.0404379101.
Walker MB, Kimmel CB. 2007. A two-color acid-free cartilage and bone stain for zebrafish larvae. Biotech Histochem 82(1):23–28, PMID: 17510811, https://doi.org/10.1080/10520290701333558.
West JA, Davis CP, Sunwoo H, Simon MD, Sadreyev RI, Wang PI, et al. 2014. The long noncoding RNAs NEAT1 and MALAT1 bind active chromatin sites. Mol Cell 55(5):791–802, PMID: 25155612, https://doi.org/10.1016/j.molcel.2014.07.012.
Westerfield M. 2000. *The Zebrafish Book. A Guide for the Laboratory Use of Zebrafish (Danio rerio)*. 4th ed. Eugene, OR: University of Oregon.
Westerfield M. 2007. *The Zebrafish Book. A Guide for the Laboratory Use of Zebrafish (Danio rerio)*. 5th ed. Eugene, OR: University of Oregon Press.
Wickham H. 2016. *Ggplot2: Elegant Graphics for Data Analysis*. New York: Springer-Verlag.
Wincent E, Stegeman JJ, Jönsson ME. 2015. Combination effects of AHR agonists and Wnt/β-catenin modulators in zebrafish embryos: implications for physiological and toxicological AHR functions. Toxicol Appl Pharmacol 284(2):163–179, PMID: 25711857, https://doi.org/10.1016/j.taap.2015.02.014.
Xiong KM, Peterson RE, Heideman W. 2008. Aryl hydrocarbon receptor-mediated down-regulation of sox9b causes jaw malformation in zebrafish embryos. Mol Pharmacol 74(6):1544–1553, PMID: 18784347, https://doi.org/10.1124/mol.108.050435.
Yan B, Liu S, Shi Y, Liu N, Chen L, Wang X, et al. 2018. Activation of AhR with nuclear IKKα regulates cancer stem-like properties in the occurrence of radioresistance. Cell Death Dis 9(5):490, PMID: 29706625, https://doi.org/10.1038/s41419-018-0542-9.
Yan YL, Willoughby J, Liu D, Crump JG, Wilson C, Miller CT, et al. 2005. A pair of Sox: distinct and overlapping functions of zebrafish sox9 co-orthologs in craniofacial and pectoral fin development. Development 132(5):1069–1083, PMID: 15689370, https://doi.org/10.1242/dev.01674.
Ye M, Zhang Y, Gao H, Xu Y, Jing P, Wu J, et al. 2018. Activation of the aryl hydrocarbon receptor leads to resistance to EGFR TKIs in non-small cell lung cancer by activating Src-mediated bypass signaling. Clin Cancer Res 24(5):1227–1239, PMID: 29229632, https://doi.org/10.1158/1078-0432.CCR-17-0396.
Yue F, Cheng Y, Breschi A, Vierstra J, Wu W, Ryba T, et al. 2014. A comparative encyclopedia of DNA elements in the mouse genome. Nature 515(7527):355–364, PMID: 25409824, https://doi.org/10.1038/nature13992.
Zeileis A. 2004. Econometric computing with HC and HAC covariance matrix estimators. J Statistical Software 11:1–17, https://doi.org/10.18637/jss.v011.i10.
Zeileis A. 2006. Object-oriented computation of sandwich estimators. J Statistical Software 16:1–16, https://doi.org/10.18637/jss.v016.i09.